AD-A163 178 CURVATURE EFFECTS OF THREE-DIMENSIONAL THICK STERN BOUNDARY LAYERS(U) DAVID W TAYLOR NAVAL SHIP RESEARCH AND DEVELOPMENT CENTER BETHESDA MD Y LEE ET AL. DEC 85 1/1

UNCLASSIFIED DTNSRDC-85/087 F/G 20/4 NL

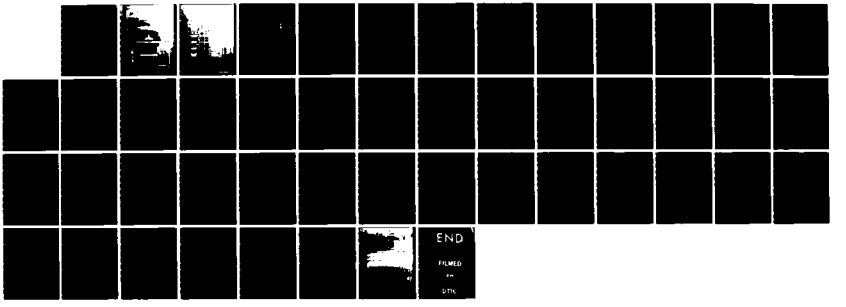

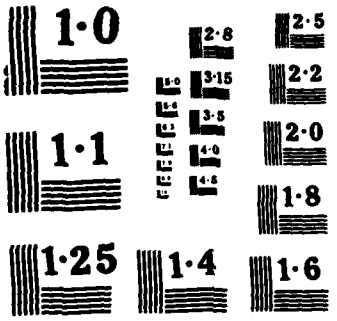

NATIONAL BUREAU OF STANDARDS
MICROCOPY RESOLUTION TEST CHART

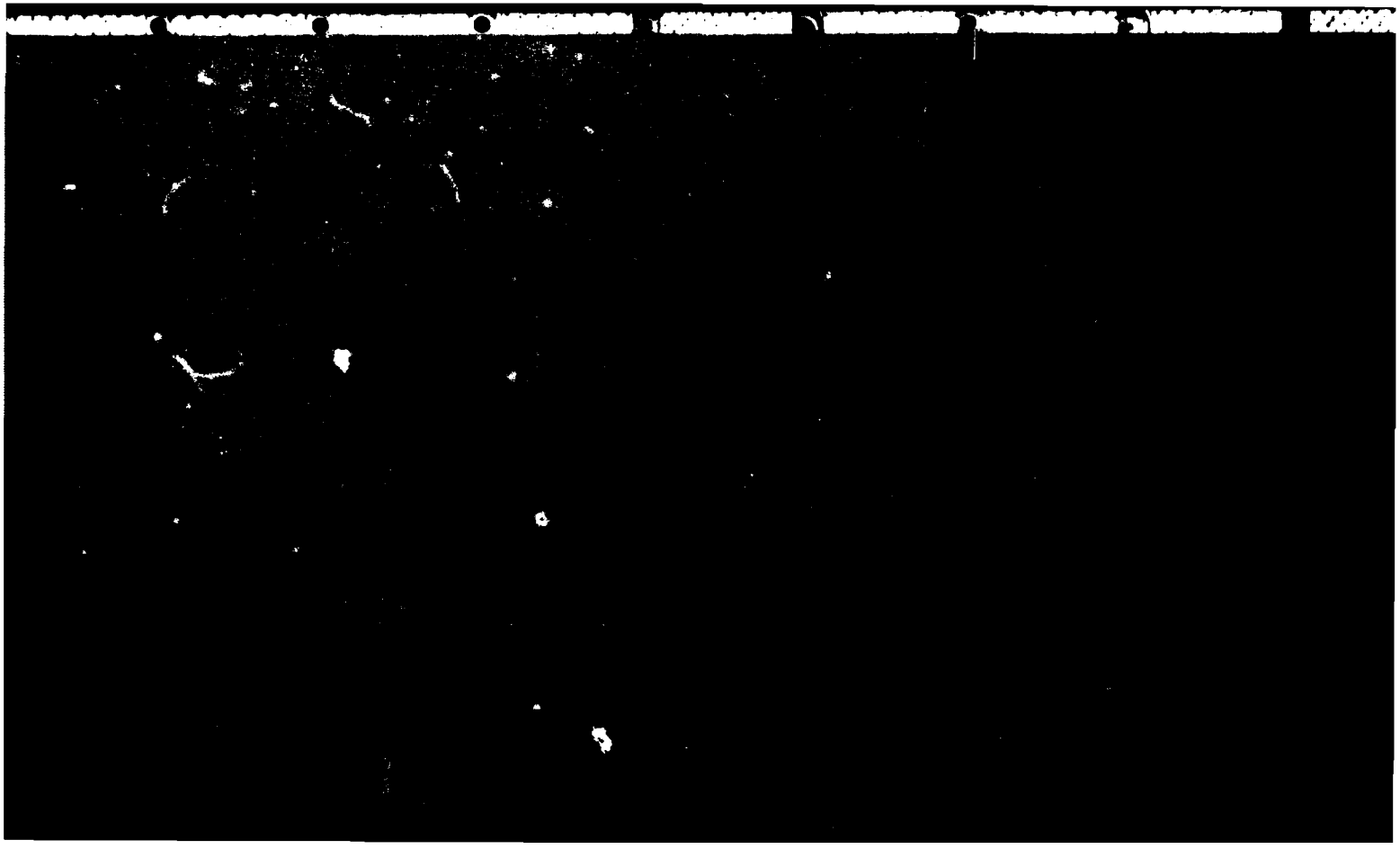

UNCLASSIFIED

SECURITY CLASSIFICATION OF THIS PAGE

AD-A163 178

REPORT DOCUMENTATION PAGE

1a REPORT SECURITY CLASSIFICATION UNCLASSIFIED	1b RESTRICTIVE MARKINGS
2a SECURITY CLASSIFICATION AUTHORITY	3 DISTRIBUTION / AVAILABILITY OF REPORT Approved for Public Release; Distribution is Unlimited.
2b DECLASSIFICATION / DOWNGRADING SCHEDULE	
4 PERFORMING ORGANIZATION REPORT NUMBER(S) DTNSRDC-85/087	5 MONITORING ORGANIZATION REPORT NUMBER(S)
6a NAME OF PERFORMING ORGANIZATION David Taylor Naval Ship R&D Center 6b OFFICE SYMBOL (If applicable) 1542	7a NAME OF MONITORING ORGANIZATION
6c ADDRESS (City, State, and ZIP Code) Bethesda, MD 20084-5000	7b ADDRESS (City, State, and ZIP Code)
8a NAME OF FUNDING / SPONSORING ORGANIZATION 8b OFFICE SYMBOL (If applicable)	9 PROCUREMENT INSTRUMENT IDENTIFICATION NUMBER
8c ADDRESS (City, State, and ZIP Code)	10 SOURCE OF FUNDING NUMBERS

PROGRAM ELEMENT NO	PROJECT NO	TASK NO	WORK UNIT ACCESSION NO
61153N		SR0230101	DN678154

DTIC ELECTE JAN 17 1986 D A

11 TITLE (Include Security Classification)

CURVATURE EFFECTS OF THREE-DIMENSIONAL THICK STERN BOUNDARY LAYERS

12 PERSONAL AUTHOR(S)

Lee Yu-Tai and Chang Ming Shun

13a TYPE OF REPORT	13b TIME COVERED FROM ____ TO ____	14 DATE OF REPORT (Year, Month, Day)	15 PAGE COUNT
FINAL		1985, December	44

16 SUPPLEMENTARY NOTATION

→ Keywords:

17 COSATI CODES		
FIELD	GROUP	SUB-GROUP

18 SUBJECT TERMS (Continue on reverse if necessary and identify by block number)

→Thick turbulent stern flows; longitudinal and transverse curvature effects; turbulence modeling; eddy viscosity.

19 ABSTRACT (Continue on reverse if necessary and identify by block number)

Thick boundary-layer equations, including the variation of the metric coefficients with distance normal to the surface, are solved from the nose to the tail of an elongated three-dimensional body. Iteration between potential and boundary-layer flow solutions is adopted to obtain a converged solution in the stern region. The complete procedure makes use of Keller's box numerical scheme in a non-orthogonal curvilinear coordinate system and an isotropic eddy-viscosity model for the Reynolds stress tensor in both streamwise and crosswise directions. The numerical method allows the calculation of flows in which the crosswise component of velocity contains regions of flow reversal across the boundary layer. The inviscid pressure is determined by using the Hess-Smith method. The program is validated for an axisymmetric body, and then the calculations are compared with measurements for two three-dimensional bodies having elliptical transverse sections.

20 DISTRIBUTION / AVAILABILITY OF ABSTRACT	21 ABSTRACT SECURITY CLASSIFICATION
☒ UNCLASSIFIED UNLIMITED ☐ SAME AS RPT ☐ DTIC USERS	UNCLASSIFIED
22a NAME OF RESPONSIBLE INDIVIDUAL Lee Yu-Tai	22b TELEPHONE (Include Area Code) 202/227-1340
	22c OFFICE SYMBOL Code 1542

DD FORM 1473, 84 MAR 83 APR edition may be used until exhausted. All other editions are obsolete.

SECURITY CLASSIFICATION OF THIS PAGE

UNCLASSIFIED

TABLE OF CONTENTS

LIST OF FIGURES

LIST OF TABLES

NOTATION

a	a constant used in Eq. (37)
A	a damping factor $=\left(\frac{26\nu}{u_\tau}\right)$
C_p	pressure coefficient, $=\left(\frac{p-p_o}{\frac{1}{2}\rho U_o^2}\right)$
f, g	dimensionless potential functions, defined in Eq. (23)
G	dimensionless normal velocity, defined in Eq. (24)
h_1, h_2, h_3	metric coefficients
K_1, K_2	geometric parameters, defined in Eq. (12)
$K_{12}, K_{21}, K_{13}, K_{23}$	geodesic curvatures
ℓ	mixing length
L	total length of the body
m_1	$=\frac{1}{2}\left(1+\frac{s_1}{h_{10}u_e}\frac{\partial u_e}{\partial \xi}\right)+\frac{s_1}{h_{10}\,h_{20}\sin\alpha}\frac{\partial}{\partial \xi}\,(h_{20}\sin\alpha)$
m_{2c}	$=\frac{s_1}{h_{10}\,u_e}\frac{\partial u_e}{\partial \xi}$
m_{2d}	$=-s_1\cot\alpha\,(m_{20}/a_1+m_{21}/a_2)$
m_3	$=-s_1\frac{u_o}{u_e}\cot\alpha\,(m_{22}/a_1+m_{23}/a_2)$
m_4	$=s_1\,(m_{26}/a_1+m_{27}/a_2)$
m_{5c}	$=\frac{s_1}{h_{20}}\frac{u_o}{u_e^2}\frac{\partial u_e}{\partial \zeta}$
m_{5d}	$=s_1\frac{u_o}{u_e}\,(m_{24}/a_1+m_{25}/a_2)$

$$m_6 = \frac{s_1}{h_{10}\, h_{20} \sin\alpha}\, \frac{1}{\sqrt{u_e s_1}}\, \frac{\partial}{\partial \zeta}\left(\sqrt{u_e s_1}\, h_{10} \sin\alpha\, \frac{u_o}{u_e}\right)$$

$$m_7 = \frac{s_1}{h_{20}}\, \frac{u_o}{u_e}$$

$$m_8 = s_1\left(\frac{u_o}{u_e}\right)^2 \csc\alpha\, (m_{22}/\alpha_1 + m_{23}/\alpha_2)$$

$$m_9 = s_1\left(\frac{u_e}{u_o}\right)^2 \csc\alpha\, (m_{20}/\alpha_1 + m_{21}/\alpha_2)$$

$$m_{10} = s_1/h_{10}$$

$$m_{11} = (m_{2c}/\alpha_{1e} - m_{2de}) + \frac{w_e}{u_o}\left(\frac{m_{5c}}{\alpha_{2e}} + m_{5de}\right) + \left(\frac{w_e}{u_o}\right)^2 m_{8e} - \frac{m_{13e}}{\alpha_{1e}\,\alpha_{2e}}\, \tilde{G}_e + \left(\frac{m_{15}}{\alpha_{1e}} + \frac{m_{16}}{\alpha_{2e}}\, \frac{w_e}{u_o}\right) \eta_e\, \tilde{v}_e$$

$$m_{12} = m_{4e}\frac{w_e}{u_o} + m_{3e}\left(\frac{w_e}{u_o}\right)^2 + m_{9e} + \frac{m_{10}}{\alpha_{1e}}\, \frac{\partial}{\partial \xi}\left(\frac{w_e}{u_o}\right) + \frac{m_7}{\alpha_{2e}}\, \frac{w_e}{u_o}\, \frac{\partial}{\partial \zeta}\left(\frac{w_e}{u_o}\right) - \frac{w_e}{u_o}\, \frac{m_{14e}}{\alpha_{1e}\,\alpha_{2e}}\, \tilde{G}_e + \left(\frac{m_{15}}{\alpha_{1e}} + \frac{m_{16}}{\alpha_{2e}}\, \frac{w_e}{u_o}\right) \eta_e\, \tilde{t}_e$$

$$m_{130} = K_{130}\sqrt{\nu s_1/u_e}$$

$$m_{13} = m_{130}/\alpha_1$$

$$m_{140} = K_{230}\sqrt{\nu s_1/u_e}$$

$$m_{14} = m_{140}/\alpha_2$$

$$m_{15} = \frac{s_1^2}{2h_{10}}\, \frac{1}{u_e}\, \frac{\partial}{\partial \xi}\left(\frac{u_e}{s_1}\right)$$

$$m_{16} = \frac{s_1^2}{2h_{20}}\, \frac{u_o}{u_e^2}\, \frac{\partial}{\partial \zeta}\left(\frac{u_e}{s_1}\right)$$

$$m_{17} = m_7\, \frac{\partial m_{130}}{\partial \zeta}$$

$$m_{18} = m_{10}\, \frac{\partial m_{140}}{\partial \xi}$$

$$m_{20} = \frac{1}{h_{10}\, h_{20} \sin\alpha}\, \frac{\partial}{\partial \xi}\, (h_2 \cos\alpha)$$

m_{21}	$= -\dfrac{1}{h_{10}\, h_{20} \sin \alpha} \dfrac{\partial\, h_{10}}{\partial \zeta}$
m_{22}	$= -\dfrac{1}{h_{10}\, h_{20} \sin \alpha} \dfrac{\partial\, h_{20}}{\partial \xi}$
m_{23}	$= \dfrac{1}{h_{10}\, h_{20} \sin \alpha} \dfrac{\partial}{\partial \zeta} (h_1 \cos \alpha)$
m_{24}	$= 2 \cot \alpha\, m_{22}$
m_{25}	$= -(1 + \cos^2 \alpha) \csc \alpha\, m_{21}$
m_{26}	$= -(1 + \cos^2 \alpha) \csc \alpha\, m_{22}$
m_{27}	$= 2 \cot \alpha\, m_{21}$
p	fluid static pressure
p_o	reference fluid static pressure
r_o	body radius
s_1	geometric parameter, defined in Eq. (22)
u, v, w	velocity components in the x, y, z-directions
$\tilde{u}, \tilde{v}, \tilde{w}, \tilde{G}, \tilde{\tau}$	transformed variables, defined in Eq. (25)
u_t	total velocity
u_τ	shear velocity $(= \sqrt{\tau_w/\varrho})$
$\overline{u'v'}, \overline{v'w'}$	components of Reynolds stress
x, y, z	nonorthorgonal coordinates
$\bar{x}, \bar{y}, \bar{z}$	Cartesian coordinates
x_{sep}	x-value at separation
y_c	y-value at which inner and outer layer eddy viscosity regions connect
α	angle between x- and z-coordinates
α_1, α_2	geometric parameters, defined in Eq. (6)
γ_{tr}	an intermittency factor in transition region, defined in [11]
δ	boundary layer thickness

δ_p^*	planar displacement thickness ($= \int_0^\delta (1-u_t/u_{te})\, dy$)
ε_m	turbulent eddy viscosity, defined in Eq. (16)
θ	azimuthal angle, defined in Fig. 3
θ_{sep}	θ-value at separation
ν	kinematic viscosity
ξ, ζ, η	transformed coordinates
ρ	fluid density
τ_w	wall shear stress
τ_x, τ_z	shear stress, defined in Eq. (12)
ϕ, ψ	vector potentials, defined in Eq. (23)

Subscripts

e	at $y = \delta$
o, w	at the surface
s	in the streamline direction

ABSTRACT

Thick boundary-layer equations, including the variation of the metric coefficients with distance normal to the surface, are solved from the nose to the tail of an elongated three dimensional body. Iteration between potential and boundary-layer flow solutions is adopted to obtain a converged solution in the stern region. The complete procedure makes use of Keller's box numerical scheme in a non-orthogonal curvilinear coordinate system and an isotropic eddy-viscosity model for the Reynolds stress tensor in both streamwise and crosswise directions. The numerical method allows the calculation of flows in which the crosswise component of velocity contains regions of flow reversal across the boundary layer. The inviscid pressure is determined by using the Hess-Smith method. The program is validated for an axisymmetric body and then the calculations are compared with measurements for two three-dimensional bodies having elliptical transverse sections.

ADMINISTRATIVE INFORMATION

This research was funded by the General Hydrodynamics Research Program, Program Element 61153N, Task Area SRO230101, DTNSRDC Work Unit 1542-070.

INTRODUCTION

When compared to the thin hull boundary layer, much less progress has been made in the prediction of the three-dimensional (3-D) thick stern turbulent boundary layer and wake which involve higher-order effects. Only three out of the seventeen prediction methods in the SSPA ITTC 1980 Ship Boundary Layer Workshop[1]*considered higher-order effects. This is because of (a) the complexity of the 3-D flow, and (b) the existence of flow separation and trailing vorticity. Complete computational solutions of the full Navier-Stokes equations are still limited to laminar time averaged turbulent flows. These computations require the use of computers having large core memories and high speed processors. Seeking solutions for higher-order equations, whose complexity lies somewhere between that of the Reynolds and the thin boundary layer equations for turbulent flow, is a current on-going research topic in computational ship hydrodynamics.

Two different approaches exist for solving higher order equations. The first approach simplifies the Reynolds equations by discarding the terms related to streamwise diffusion. The resulting equations are called the partially parabolic equations. Examples of this approach are contained in References 2, 3, and 4. The second approach generalizes the first order boundary layer equations by introducing terms related to the second-order curvature effects. The complete solution procedure includes viscous inviscid interaction to account for deficiencies in the governing equations as well as in the numerical solution techniques. This approach has been widely used by the aircraft industry; applications to ship flows are

*A complete listing of references is given on page 33.

given in References 5 and 6. The parabolic nature of the equations comprising the latter approach indicates the downstream pressure field does not influence upstream flow characteristics. Through the viscid-inviscid interaction process, the solutions are corrected by successive global iterations. Although Abdelmequid et al.[2] has made some comparisons between the two approaches, he unfortunately adopted the second approach without including interactions. It is still not known which approach gives better predictions.

In this paper, the numerical method of Cebeci et al.[7] for solving 3-D boundary layers is expanded to include the curvature terms for thick stern boundary layers. Several new geometrical parameters are introduced by using the original nonorthogonal coordinate system. The boundary conditions at the edge of the thick boundary layer are updated in the global iterations between viscous and inviscid solutions. Some encouraging results have been obtained for an axisymmetric flow and two 3-D flows with separation. In their survey of boundary-layer theory for flow with separation, McDonald and Briley[8] concluded that 2-D flows with mild separation can be treated by applying an interaction procedure to the boundary-layer equations. The present results shed some light on extending this approach to 3-D flows.

COORDINATE SYSTEM

A curvilinear nonorthogonal surface-fitted coordinate system is used to represent ship-hull surfaces. Figure 1 depicts this coordinate system (x, y, z) along with Cartesian coordinates ($\bar{x}$, $\bar{y}$, $\bar{z}$). Here, α is the angle between x and z, and y is normal to the hull surface. The potential flow solution for a ship hull is solved in terms of the Cartesian coordinates and the boundary-layer equations are expressed in the (x, y, z) coordinate system. We select $x = \bar{x}$, and z lies in the $\bar{y}\bar{z}$-plane. Because the coordinate system is nonorthogonal, we are free to select the value of z in the plane to satisfy the condition that the boundary line of the ship hull is coincident with the z = constant coordinate line. In this paper, z is determined by mapping each $\bar{y}\bar{z}$ crossplane into a half-unit circle by the numerical method developed by Halsey[9]. The polar angle, normalized by π on the unit circle, is taken as the z-value. The z-values then range from 0 to 1 on each crossplane. The advantage of the mapping method is that equi-interval, z = constant, coordinate lines are automatically concentrated in the region of large curvature where the boundary layer characteristics are expected to vary greatly.

In this nonorthogonal coordinate system, the geodesic curvatures of the curves, z = constant, in the direction of x and the curves x = constant in the direction of z are given in Reference 7 as

$$K_{1} = \frac{1}{h_1 h_3 \sin\alpha}\left[\frac{\partial}{\partial x}(h_3 \cos\alpha) - \frac{\partial h_1}{\partial z}\right] \qquad (1)$$

$$K_{2} = \frac{1}{h_1 h_3 \sin\alpha}\left[\frac{\partial}{\partial z}(h_1 \cos\alpha) - \frac{\partial h_3}{\partial x}\right]$$

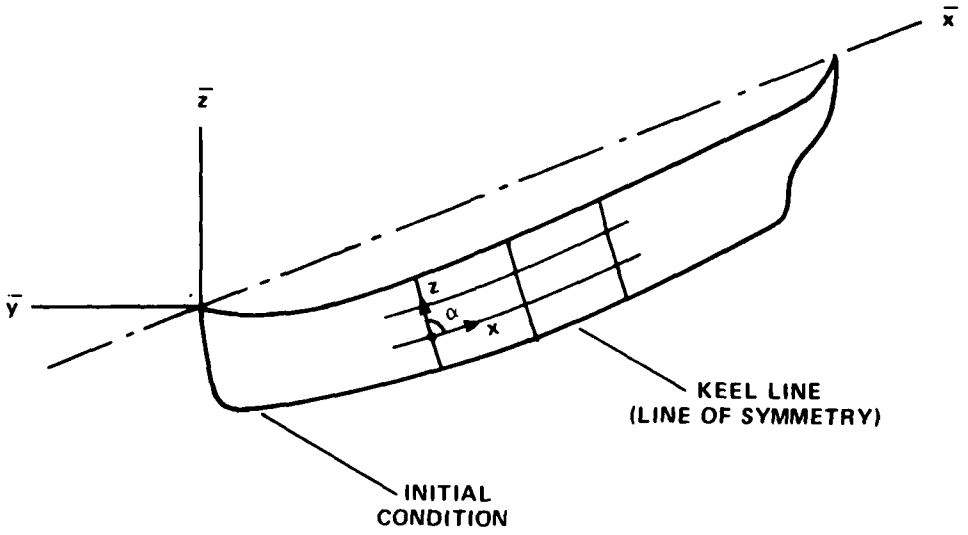

Figure 1 — Coordinate System

and the geodesic curvatures of the curves, y = constant, in the directions of x and z are

$$K_{13} = \frac{1}{h_1} \frac{\partial h_1}{\partial y}$$
$$K_{23} = \frac{1}{h_2} \frac{\partial h_2}{\partial y} \tag{2}$$

Since y is selected to be normal to the hull surface, the metric coefficient h_3 can be chosen as unity. Along the x and z directions, h_1 and h_2 are, in general, functions of x,y, and z; that is

$$h_1 = h_1 (x, y, z)$$
$$h_2 = h_2 (x, y, z)$$

Expanding h_1 and h_2 in series about the coordinate origin leads to

$$h_1 = h_{10} \left[1 + y \left(\frac{1}{h_1} \frac{\partial h_1}{\partial y} \right)_{y = 0} + \ldots \right]$$
$$h_2 = h_{20} \left[1 + y \left(\frac{1}{h_2} \frac{\partial h_2}{\partial y} \right)_{y = 0} + \ldots \right] \tag{3}$$

where h_{10} and h_{20} are the corresponding values at the surface and are given in Reference 7.

$$h_{10} = \left[1 + \left(\frac{\partial \bar{y}}{\partial x} \right)^2 + \left(\frac{\partial \bar{z}}{\partial x} \right)^2 \right]^{1/2}$$
$$h_{20} = \left[\left(\frac{\partial \bar{y}}{\partial z} \right)^2 + \left(\frac{\partial \bar{z}}{\partial z} \right) \right]^{1/2} \tag{4}$$

By comparing Equation (3) to Equation (2) and dropping the higher order terms in the series expansion, we can write

$$h_1 = h_{10} \alpha_1 \quad , \quad h_2 = h_{20} \alpha_2 \tag{5}$$

α_1 and α_2 are defined as

$$\alpha_1 = 1 + K_{130}\, y \quad , \quad \alpha_2 = 1 + K_{230}\, y \tag{6}$$

where K_{130} and K_{230} are the surface curvatures of K_{13} and K_{23}. Substitution of Equation (5) into Equation (2) results in

$$K_{13} = \frac{K_{130}}{\alpha_1} \quad , \quad K_{23} = \frac{K_{230}}{\alpha_2} \tag{7}$$

The other related geometric parameters are given in Reference 7.

GOVERNING EQUATIONS

BOUNDARY-LAYER EQUATIONS

The governing second-order boundary-layer equations for a steady, incompressible, laminar or turbulent flow in the present curvilinear nonorthogonal coordinate system are given[7,10] by:

Continuity Equation

$$\frac{\partial}{\partial x}(u h_2 \sin\alpha) + \frac{\partial}{\partial z}(w h_1 \sin\alpha) + \frac{\partial}{\partial y}(v h_1 h_2 \sin\alpha) = 0 \tag{8}$$

x-Momentum Equation

$$\begin{aligned} &\frac{u}{h_1}\frac{\partial u}{\partial x} + \frac{w}{h_2}\frac{\partial u}{\partial z} + v\frac{\partial u}{\partial y} - K_{12}\, u^2 \cot\alpha + K_{21}\, w^2 \csc\alpha + K_1\, uw + K_{13}\, uv \\ &\quad = -\frac{\csc^2\alpha}{h_1}\frac{\partial}{\partial x}\left(\frac{p}{\varrho}\right) + \frac{\cot\alpha \csc\alpha}{h_2}\frac{\partial}{\partial z}\left(\frac{p}{\varrho}\right) + \frac{1}{h_1 h_2}\frac{\partial}{\partial y}(h_1 h_2 \tau_x) \end{aligned} \tag{9}$$

z-Momentum Equation

$$\begin{aligned} &\frac{u}{h_1}\frac{\partial w}{\partial x} + \frac{w}{h_2}\frac{\partial w}{\partial z} + v\frac{\partial w}{\partial y} - K_{21}\, w^2 \cot\alpha + K_{12}\, u^2 \csc\alpha + K_2\, uw + K_{23}\, wv \\ &\quad = \frac{\cot\alpha \csc\alpha}{h_1}\frac{\partial}{\partial x}\left(\frac{p}{\varrho}\right) - \frac{\csc^2\alpha}{h_2}\frac{\partial}{\partial z}\left(\frac{p}{\varrho}\right) + \frac{1}{h_1 h_2}\frac{\partial}{\partial y}(h_1 h_2 \tau_z) \end{aligned} \tag{10}$$

y-Momentum Equation

$$\frac{u}{h_1}\frac{\partial v}{\partial x} + \frac{w}{h_2}\frac{\partial v}{\partial z} + v\frac{\partial v}{\partial y} - K_{13}u^2 - K_{23}w^2 = -\frac{\partial}{\partial y}\left(\frac{p}{\varrho}\right) \tag{11}$$

where the parameters K_1, K_2, τ_x, and τ_z are defined by

$$K_1 = \frac{1}{\sin\alpha}\left[-\left(K_{12} + \frac{1}{h_1}\frac{\partial\alpha}{\partial x}\right) + \cos\alpha\left(K_{21} + \frac{1}{h_2}\frac{\partial\alpha}{\partial z}\right)\right]$$

$$K_2 = \frac{1}{\sin\alpha}\left[-\left(K_{21} + \frac{1}{h_2}\frac{\partial\alpha}{\partial z}\right) + \cos\alpha\left(K_{12} + \frac{1}{h_1}\frac{\partial\alpha}{\partial x}\right)\right] \tag{12}$$

$$\frac{\tau_x}{\varrho} = \nu\frac{\partial u}{\partial y} - \overline{u'v'}\ ,\ \frac{\tau_z}{\varrho} = \nu\frac{\partial w}{\partial y} - \overline{v'w'}$$

and u, v, and w represent the velocity components in the x, y, and z directions, respectively. The parameters p, ϱ and ν are the fluid static pressure, density, and kinematic viscosity; $\varrho\overline{u'v'}$ and $\varrho\overline{v'w'}$ are Reynolds stresses. The non-slip boundary condition is applied at the wall, i.e., y = 0. At the edge of the boundary layer, i.e., y = δ, Equations (9) to (11) can be written as

$$\frac{u_e}{h_{1e}}\frac{\partial u_e}{\partial x} + \frac{w_e}{h_{2e}}\frac{\partial u_e}{\partial z} - K_{12e}u_e^2\cot\alpha + K_{21e}w_e^2\csc\alpha + K_{13e}u_e v_e + K_{1e}u_e w_e$$

$$= -\frac{\csc^2\alpha}{h_{1e}}\frac{\partial}{\partial x}\left(\frac{p}{\varrho}\right)_e + \frac{\cot\alpha\csc\alpha}{h_{2e}}\frac{\partial}{\partial z}\left(\frac{p}{\varrho}\right)_e \tag{13}$$

$$\frac{u_e}{h_{1e}}\frac{\partial w_e}{\partial x} + \frac{w_e}{h_{2e}}\frac{\partial w_e}{\partial z} - K_{21e}w_e^2\cot\alpha + K_{12e}u_e^2\csc\alpha + K_{2e}u_e w_e + K_{23e}w_e v_e$$

$$= \frac{\cot\alpha\csc\alpha}{h_{1e}}\frac{\partial}{\partial x}\left(\frac{p}{\varrho}\right)_e - \frac{\csc^2\alpha}{h_{2e}}\frac{\partial}{\partial z}\left(\frac{p}{\varrho}\right)_e \tag{14}$$

$$\frac{u_e}{h_{1e}}\frac{\partial v_e}{\partial x} + \frac{w_e}{h_{2e}}\frac{\partial v_e}{\partial z} + v_e\frac{\partial v_e}{\partial y} - K_{13e}u_e^2 - K_{23e}w_e^2 = -\frac{\partial}{\partial y}\left(\frac{p}{\varrho}\right)_e \tag{15}$$

Thus at $y = \delta$, the pressure gradient terms can be expressed in terms of u_e, v_e and w_e. In the numerical examples shown later, the boundary-layer Equations (9), (10), (13), and (14) are solved simultaneously through the procedures described in the following sections.

TURBULENCE CLOSURE

Cebeci-Smith Eddy-Viscosity Model

Solutions of Equations (9) and (10) require some parameterization of the shear stresses τ_x and τ_z. Cebeci[7] used an isotropic eddy-viscosity concept for his 3-D computation. These 3-D formulas are given as

$$-\overline{u'v'} = \varepsilon_m \frac{\partial u}{\partial y} \quad , \quad -\overline{v'w'} = \varepsilon_m \frac{\partial w}{\partial y} \tag{16}$$

The eddy viscosity ε_m is divided into the inner and outer layers. They are continuously connected at $y = y_c$, where $(\varepsilon_m)_i = (\varepsilon_m)_o$. In the inner region, $(\varepsilon_m)_i$ is defined as

$$(\varepsilon_m)_i = \ell^2 \left[\left(\frac{\partial u}{\partial y} \right)^2 + \left(\frac{\partial w}{\partial y} \right)^2 + 2 \cos \alpha \left(\frac{\partial u}{\partial y} \right) \left(\frac{\partial w}{\partial y} \right) \right]^{1/2} \gamma_{tr} \tag{17}$$

where ℓ is a mixing-length approximation equal to 0.4 y [1-exp(1-y/A)], A is a damping factor equal to $26\nu/u_\tau$, and u_τ is the shear velocity. Also γ_{tr} is an intermittency factor to account for the turbulent and nonturbulent flows produced by the fluctuating outer edge of the boundary layer, and is defined in Reference 11. In the outer region, $(\varepsilon_m)_o$ becomes

$$(\varepsilon_m)_o = 0.0168 \, u_{te} \, \delta_p^* \, \gamma_{tr} \tag{18}$$

where δ_p^* is the planar displacement thickness and u_{te} is the total velocity at $y = \delta$.

Modified Eddy-Viscosity Model

In order to calculate a thick 3-D boundary layer by means of the eddy-viscosity concept, it is necessary to include the curvature effect[12] in the eddy-viscosity formulations. In the appendix, a formula is derived to modify the inner eddy-viscosity, Equation (17), by

$$(\varepsilon_m)_i = \alpha_1 \alpha_2 \ell^2 \frac{\partial u_s}{\partial y} \gamma_{tr} \tag{19}$$

where

$$\ell = \begin{cases} \dfrac{0.4}{K_{230}-K_{130}} \ln\left(\dfrac{\alpha_2}{\alpha_1}\right)\left\{1 - \exp\left[-\dfrac{\ln \alpha_2/\alpha_1}{(K_{230}-K_{130})A}\right]\right\}, & \alpha_1 \neq \alpha_2 \\ \dfrac{0.4\ y}{\alpha_1}\left\{1 - \exp\left(-\dfrac{y}{\alpha_1 A}\right)\right\}, & \alpha_1 = \alpha_2 \end{cases} \tag{20}$$

For the outer-layer eddy viscosity, a constant value 0.0168 was used in Cebeci's original model, as shown in Equation (18). This has been proved to be inadequate for a thick turbulent boundary layer[13,14]. A suggested revised form was proposed for an axisymmetric case in Reference 14. For a simple extension of Reference 14, the following formulas are used to account for the curvature effect on the outer-layer eddy viscosity when $K_{230}\,\delta \geq 0.2$.

$$(\epsilon_m)_o = {}_F{}^2\,(0.0168) u_{te} \delta_p^* \gamma_{tr} \tag{21}$$

where

$$\ell_F = \frac{\sqrt{(1+0.6\ K_{230}\,\delta)^2 - 1}}{2.522\ K_{230}\,\delta}$$

The value of ℓ_F becomes $\sqrt{(r_o+0.6\delta)^2 - r_o{}^2}/2.522\delta$ for the axisymmetric thick boundary layer, a formula originally proposed by Huang et al.[13,14]

Huang's Eddy-Viscosity Model

From three sets of measurements[13,15,16] for one axisymmetric and two 3-D bodies, Huang has obtained a single correlation[17] to represent the eddy viscosity distribution in 3-D thick-stern boundary layers. Huang's turbulence model is used as a two-layer isotropic eddy-viscosity model. It preserves the Cebeci-Smith inner-layer eddy viscosity, as shown in Equation (17). The outer-layer eddy viscosity uses Equation (18) unless $A_F/A \geq 1.513$ and $\delta K_{230} \geq 0.23$, where A_F is the effective turbulence area defined in Reference 17 as 60% of the flow passage area and A is the cross-sectional area at the same axial location. In order to accommodate the present numerical method described in the later section, a constant eddy viscosity selected for the entire outer layer is given by

$$(\varepsilon_m)_o = \text{Max} \left\{ \ell^2 \left[\left(\frac{\partial u}{\partial y}\right)^2 + \left(\frac{\partial w}{\partial y}\right)^2 + 2\cos\alpha \left(\frac{\partial u}{\partial y}\right)\left(\frac{\partial w}{\partial y}\right) \right]^{1/2} \right\}$$

where

$$\ell = 0.169 \sqrt{A_F/\pi}\,(y/\delta) \exp[-1.2(y/\delta) - 1.0667(y/\delta)^3]$$

TRANSFORMED BOUNDARY-LAYER EQUATIONS

The boundary-layer Equations (8) to (10) are solved in the form of transformed equations by using the following transformed variables:

$$\xi = x \quad , \quad \zeta = z \quad , \quad d\eta = \sqrt{\frac{u_e}{\nu s_1}}\, dy \quad , \quad s_1 = \int_0^x h_1\, dx \tag{22}$$

A two-component vector potential, which satisifies continuity, Equation (8), is defined as

$$\psi = \sqrt{\nu s_1 u_e}\, h_{20} \sin\alpha\, f(\xi, \zeta, \eta)$$

$$\phi = \sqrt{\nu s_1 u_e}\, \frac{u_o}{u_e}\, h_{10} \sin\alpha\, g(\xi, \zeta, \eta) \tag{23}$$

where u_o is the ship speed. Accordingly, the three velocity components in the momentum equations can be cast as

$$\frac{u}{u_e} = \frac{f'}{\alpha_2} \quad , \quad \frac{w}{u_o} = \frac{g'}{\alpha_1} \quad , \quad v = -\frac{1}{\alpha_1 \alpha_2} \sqrt{\frac{\nu u_e}{s_1}}\, G$$

with

$$G = m_1 f + m_6 g + m_{10} \frac{\partial f}{\partial \xi} + m_7 \frac{\partial g}{\partial \zeta} + m_{15}\eta f' + m_{16}\eta g' \tag{24}$$

Here, primes denote differentiation with respect to η, and all the coefficients $m_i (i = 1, 2, \ldots, 27)$ are defined in the notation section.

In order to further reduce the complexity of the boundary-layer equations, we introduce the following parameters to replace the dependent variables.

$$\begin{aligned}
\tilde{u} &= \frac{u}{u_e} = \frac{f'}{\alpha_2} \quad , \qquad \tilde{v} = \left(\frac{f'}{\alpha_2}\right)' = \tilde{u}' \\
\tilde{w} &= \frac{w}{u_e} = \frac{g'}{\alpha_1} \quad , \qquad \tilde{t} = \left(\frac{g'}{\alpha_1}\right)' = \tilde{w}' \\
\tilde{G} &= G
\end{aligned} \tag{25}$$

By using the transformed Equations (22) to (25), the boundary-layer equations are finally written as five first-order partial differential equations, given as:

x-Momentum Equation

$$\begin{aligned}
&(\alpha_1\alpha_2 b\tilde{v})' + (\tilde{v} + m_{13}\tilde{u})\,\tilde{G} - \alpha_2(m_{2c} - \alpha_1 m_{2d})\,\tilde{u}^2 - \alpha_1\alpha_2 m_8\tilde{w}^2 \\
&\quad - \alpha_2\eta m_{15}\tilde{u}\tilde{v} - \alpha_1\eta m_{16}\tilde{v}\tilde{w} - \alpha_1(m_{5c} + \alpha_2 m_{5d})\,\tilde{u}\tilde{w} \\
&\quad + \alpha_1\alpha_2 m_{11} = \alpha_2 m_{10}\tilde{u}\frac{\partial\tilde{u}}{\partial\xi} + \alpha_1 m_7\tilde{w}\frac{\partial\tilde{u}}{\partial\zeta}
\end{aligned} \tag{26}$$

z-Momentum Equation

$$\begin{aligned}
&(\alpha_1\alpha_2 b\tilde{t})' + (\tilde{t} + m_{14}\tilde{w})\,\tilde{G} - \alpha_1\alpha_2 m_9\,\tilde{u}^2 - \alpha_1\alpha_2 m_3\tilde{w}^2 \\
&\quad - \alpha_2\eta m_{15}\tilde{u}\tilde{t} - \alpha_1\eta m_{16}\tilde{t}\tilde{w} - \alpha_1\alpha_2 m_4\tilde{u}\tilde{w} \\
&\quad + \alpha_1\alpha_2 m_{12} = \alpha_2 m_{10}\tilde{u}\frac{\partial\tilde{w}}{\partial\xi} + \alpha_1 m_7\tilde{w}\frac{\partial\tilde{w}}{\partial\zeta}
\end{aligned} \tag{27}$$

Continuity Equation

$$\begin{aligned}
&\tilde{G}' - [\alpha_2(m_1 + m_{15}) + \eta(m_{140}m_{15} + m_{18})]\,\tilde{u} \\
&\quad - [\alpha_1(m_6 + m_{16}) + \eta(m_{130}m_{16} + m_{17})]\,\tilde{w} - \alpha_2 m_{15}\eta\tilde{v} \\
&\quad - \alpha_1 m_{16}\eta\tilde{t} = \alpha_2 m_{10}\frac{\partial\tilde{u}}{\partial\xi} + \alpha_1 m_7\frac{\partial\tilde{w}}{\partial\zeta}
\end{aligned} \tag{28}$$

and

$$\tilde{u}' = \tilde{v} \tag{29}$$

$$\tilde{w}' = \tilde{t} \tag{30}$$

where b is the dimensionless eddy viscosity and is equal to $1+\varepsilon_m/\upsilon$. The nonslip conditions at the surface are transformed to $\tilde{u} = \tilde{w} = \tilde{G} = 0$. The conditions at the edge of the boundary layer require $\tilde{u} = 1$ and $\tilde{w} = w/u_o$. Equations (13) and (14) for the pressure gradients at the boundary-layer edge are embedded in the parameters m_{11} and m_{12}.

EQUATIONS ALONG THE KEEL LINE

In Figure 1, the keel line is identified as the line of symmetry. For a double model, the water line also becomes a symmetry line. On this symmetry plane, w and $\partial p/\partial z$ are zero, thus causing the z-momentum equation to be singular. However, differentiation with respect to z yields a nonsingular equation. After performing the necessary differentiation for the z-momentum equation and applying the appropriate symmetry conditions, we obtain the following equations:

Continuity Equation

$$\frac{\partial}{\partial x}(uh_2 \sin\alpha) + h_1 \sin\alpha\, w_z + \frac{\partial}{\partial y}(v\, h_1\, h_2 \sin\alpha) = 0 \tag{31}$$

x-Momentum Equation

$$\frac{u}{h_1}\frac{\partial u}{\partial x} + v\frac{\partial u}{\partial y} - K_{12}\, u^2 \cot\alpha + K_{13}\, uv = \frac{u_e}{h_{1e}}\frac{\partial u_e}{\partial x} - K_{12e}\, u_e^2 \cot\alpha + K_{13e}\, u_e\, v_e + \frac{1}{h_1\, h_2}\frac{\partial}{\partial y}(h_1\, h_2\, \tau_x) \tag{32}$$

z-Momentum Equation

$$\frac{u}{h_1}\frac{\partial w_z}{\partial x} + \frac{w_z^2}{h_2} + v\frac{\partial w_z}{\partial y} + K_2 u w_z + K_{23} w_z v + u^2\frac{\partial}{\partial z}(K_{12}\csc\alpha)$$
$$= \frac{u_e}{h_{1e}}\frac{\partial w_{ze}}{\partial x} + \frac{w_{ze}^2}{h_{2e}} + K_{2e} u_e w_{ze} + K_{23e} w_{ze} v_e + u_e^2\frac{\partial}{\partial z}(K_{12e}\csc\alpha) \quad (33)$$
$$+ \frac{1}{h_1 h_2}\frac{\partial}{\partial y}[h_1 h_2 (\tau_z)_z]$$

This set of equations can be transformed by using a similar set of transformed parameters as described in Reference 7, with the same modifications as used in the previous section. The final transformed first-order partial differential equations can be summarized as follows:

x-Momentum Equation

$$(\alpha_1\alpha_2 b\tilde{v})' + (\tilde{v} + m_{13}\tilde{u})\tilde{G} - \alpha_2(m_{2c} - \alpha_1 m_{2d})\tilde{u}^2 - \alpha_2 m_{15}\eta\tilde{u}\tilde{v}$$
$$+ \alpha_1\alpha_2 m_{11} = \alpha_2 m_{10}\tilde{u}\frac{\partial\tilde{u}}{\partial\xi} \quad (34)$$

z-Momentum Equation

$$(\alpha_1\alpha_2 b\tilde{t})' + (\tilde{t} + m_{14}\tilde{w})\tilde{G} - \alpha_1\alpha_2 m_4\tilde{u}\tilde{w} - \alpha_1 m_3\tilde{w}^2 - \alpha_1\alpha_2 m_9\tilde{u}^2$$
$$- \alpha_2 m_{15}\eta\tilde{u}\tilde{t} + \alpha_1\alpha_2 m_{12} = \alpha_2 m_{10}\tilde{u}\frac{\partial\tilde{w}}{\partial\xi} \quad (35)$$

Continuity Equation

$$\tilde{G}' - [\alpha_2(m_1 + m_{15}) - \eta(m_{140} m_{15} + m_{18})]\tilde{u} - \alpha_1 m_6\tilde{w}$$
$$- \alpha_2 m_{15}\eta\tilde{v} = \alpha_2 m_{10}\frac{\partial\tilde{u}}{\partial\xi} \quad (36)$$

The condition at the edge of the boundary layer is changed to $\tilde{w} = w_{ze}/u_o$. All the other parameters are the same as the ones for the general 3-D case except:

$$G = m_1 f + m_6 g + m_{10} \frac{\partial f}{\partial \xi} + \eta\, m_{15} f'$$

$$m_3 = m_6 = \frac{s_1}{h_{20}} \frac{u_o}{u_e}$$

$$m_9 = s_1 \frac{u_e}{u_o} \frac{\partial}{\partial \zeta} (K_{12} \csc \alpha)$$

$$m_{11} = \left(\frac{m_{2e}}{\alpha_{1e}} - m_{2de}\right) - \frac{m_{13e}\, \tilde{G}_e}{\alpha_{1e}\, \alpha_{2e}} + \frac{m_{15}}{\alpha_{1e}} \eta_e \tilde{v}_e$$

$$m_{12} = m_{4e} \frac{w_{ze}}{u_o} + \frac{m_3}{\alpha_{2e}} \left(\frac{w_{ze}}{u_o}\right)^2 + m_{9e} + \frac{m_{10}}{\alpha_{1e}} \frac{\partial}{\partial \xi} \left(\frac{w_{ze}}{u_o}\right)$$

$$- \frac{w_{ze}}{u_o} \frac{m_{14e}}{\alpha_{1e}\, \alpha_{2e}} \tilde{G}_e + \frac{m_{15}}{\alpha_{1e}} \eta_e \tilde{t}_e$$

NUMERICAL CALCULATION

NUMERICAL METHOD

Since the governing boundary-layer equations derived previously are parabolic, a numerical marching scheme is adequate for obtaining a solution. The marching process is started at an initial station in the bow region and is continued downstream. In the crossflow direction, the calculation proceeds from the keel line to the water line. The flow at the initial station was solved by assuming all $m_i = 0$ except $m_1 = 0.5$, which is a flat-plate solution. Equations (34) to (36) along the keel line are then employed to start the cross-stream sweep. Keller's box method[7] is used as the numerical solution scheme. This method is accomplished by first differencing the transformed boundary-layer Equations (26) to (30) with central differences. Newton's method is then applied to linearize the difference equations and, finally, the linearized system is solved by a block elimination method. Details of this scheme may be found in Reference 18.

The computations were carried out on the DTNSRDC CYBER 176. Typical run times were 80 s for one boundary-layer sweep on an 87 × 15 surface grid with an average of 60 normal grid points.

PROCEDURE FOR UPDATING OUTER-EDGE BOUNDARY CONDITIONS

An iterative procedure between the boundary layer solution and the potential solution is generally necessary in order to account for the strong interaction between these two regions of ship stern flows.[5,6,8] This interaction is usually considered by using the displacement body concept at $y = \delta^*$ or the equivalent-source concept at $y = 0$ (Reference 19). The disadvantage of using the former approach is

that a new grid of the displaced body must be generated for each iteration. Although the latter approach avoids the complexity of regenerating the grid for each iteration, a divergent source distribution is often encountered at the stern region. Improper treatment of this ill-behaved source distribution causes the global iteration to be divergent.[20,21] This problem becomes more serious when flow separation exists in the stern region.

In order to validate the present program for 3-D curvature effects and to avoid the problems associated with the displacement-body and equivalent-source approaches, a simple procedure was used to account for the thick boundary-layer effect. In this procedure, firstly (i) the boundary conditions at $y = \delta$ are obtained from the potential-flow solution at the body surface for the first iteration. For the second or higher iterations, these conditions are recalculated as the off-body points from the singularity distribution for the original body. The locations for applying the boundary conditions are obtained from the previous boundary-layer solutions. Secondly, (ii) the normal pressure gradient, as given by Equation (11), is solved by varying $\partial p/\partial x$ and $\partial p/\partial z$ linearly from $y = 0$ to $y = \delta$ for the curvature effect only.

COMPARISON OF EXPERIMENTAL DATA WITH NUMERICAL PREDICTIONS

Wind-tunnel test data[13,15,16] have been collected at DTNSRDC for the so-called axisymmetric Afterbody 1 and for two three-dimensional bodies of 2:1 and 3:1 elliptic cross-sections. The latter two three-dimensional bodies are generated from axisymmetric Afterbody 1 by

$$\frac{\bar{y}^2}{a} + a\,\bar{z}^2 = r_o(\bar{x}) \tag{37}$$

for an elliptic cross-section on the $\bar{y}\bar{z}$-plane; r_o is the corresponding axisymmetric radius at $\bar{x}$, and a is equal to 2 or 3, respectively, for the 2:1 or 3:1 body. A plot of cross-sections at the same x-location for these three bodies is shown in Figure 2. All three models have a length $L = 3.066$ m and were tested in a wind tunnel at a nominal speed of 30.48 m/s. Figure 3 shows the surface longitudinal and transverse curvatures of Afterbody 1 in the stern region. Since the order of magnitude of the longitudinal curvatures for the two 3-D bodies is the same as that of Afterbody 1, Figure 3 only shows, at a typical station, the transverse curvatures K_{230} in the girthwise direction, indicated by θ as defined in Figure 2, for both 3-D bodies. The 3:1 body has the least transverse curvature when θ is between 0° and 80°. It also possesses the largest K_{230} value when θ exceeds 80°, and reaches a maximum at $\theta = 90°$.

Boundary-layer computations were done first for the flow around axisymmetric Afterbody 1 in order to validate the ability of the program to include curvature effects across the boundary layer. The computations were started with laminar flow and transitioned to turbulent flow at $x/L = 0.03$. The

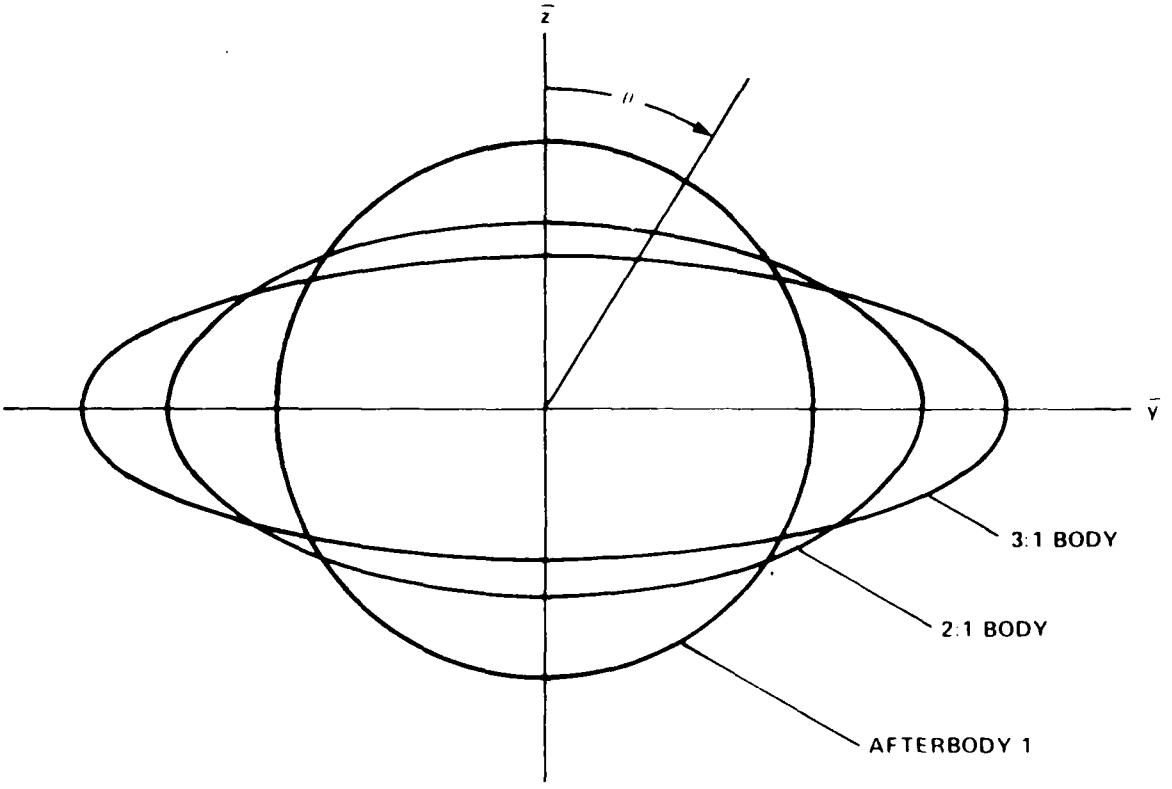

Figure 2 — Cross Sections for Three Bodies

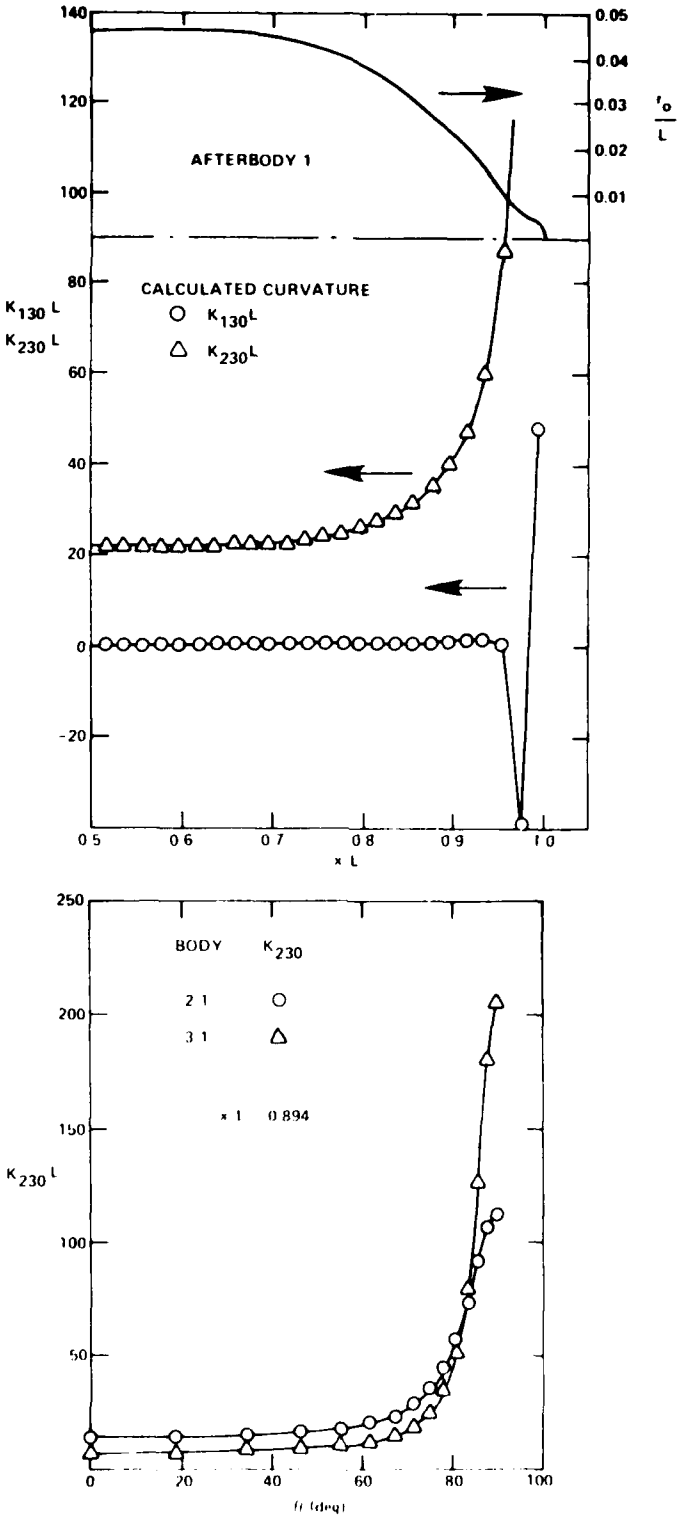

Figure 3 — Surface Curvatures of Three Bodies

pressure coefficient distribution computed from the potential flow solution for the displaced body[14] is plotted in Figure 4a as compared to the measured distribution. This calculated pressure distribution was used as the boundary condition for the following program validation runs. In Figures 4a and 4b, five sets of velocity predictions are shown along with the measured velocity profiles. These calculations are (i) 3-D thin boundary-layer calculation, indicated by $K_{13} = K_{23} = 0$ in Figure 4a; (ii) 3-D boundary-layer calculation with only transverse curvature effect, indicated by $K_{13} = 0$, K_{23} in Figure 4a; (iii) axisymmetric boundary-layer calculation[22] including only the transverse curvature, indicated by axisymmetric calculation in Figure 4b; (iv) 3-D boundary-layer calculation with both longitudinal and transverse curvature effects, indicated by K_{13}, K_{23} in Figure 4a; all the above four calculations use Cebeci-Smith turbulence closure, (v) 3-D boundary-layer calculation with both curvature effects and the modified turbulence model, indicated by K_{13}, K_{23}, and modified turbulence modeling in Figure 4a. The axisymmetric boundary-layer calculation (iii) solves the boundary-layer equations and includes the transverse curvature effect for axisymmetric flow. In terms of numerics, calculation (iii) is an exact solution of calculation (ii). Comparisons of calculation methods (ii) and (iii) are shown in Figure 4b Velocity predictions from all calculation methods, except (iii), are shown in Figure 4a. As suggested by its order of magnitude, the transverse curvature exerts a significant influence on the velocity predictions, particularly in the outer region of the viscous layer. The effect of the longitudinal curvature on the velocity prediction shows no influence at $x/L = 0.846$ and 1 to $\sim 2\%$ in the region close to the wall at $x/L = 0.934$. More importantly in this "inner region", the velocity prediction in Figure 4a using two different turbulence models (Cebeci-Smith and modified) are significantly different. The good agreement of calculations (ii) and (iii) indicates the need to include the curvature effects in 3-D boundary-layer computations. The good agreement between the predictions of calculation (v) and the measured velocity profiles suggests that the modified turbulence model gives reasonable predictions for axisymmetric flow.

Based on the findings for axisymmetric Afterbody 1, predictions of the flow about the two 3-D bodies were made for the following approximations in order to examine the significance of the curvature effects and the turbulence modeling. Thus, they are

(i) Thin boundary-layer calculation with the Cebeci-Smith model and using the calculated potential flow solution at the wall (C_{pw}) as the boundary conditions.

(ii) Thin boundary-layer calculation with the Cebeci-Smith model and using the boundary conditions (C_{pe}) obtained from the potential solution at the edge of the boundary layer.

The following three calculations use C_{pe} and the calculated values of K_{13} and K_{23} obtained from Equation (7). The boundary-layer calculations were performed by using the procedures described previously for updating the edge boundary conditions. The turbulence model for each calculation is:

(iii) Cebeci Smith turbulence model

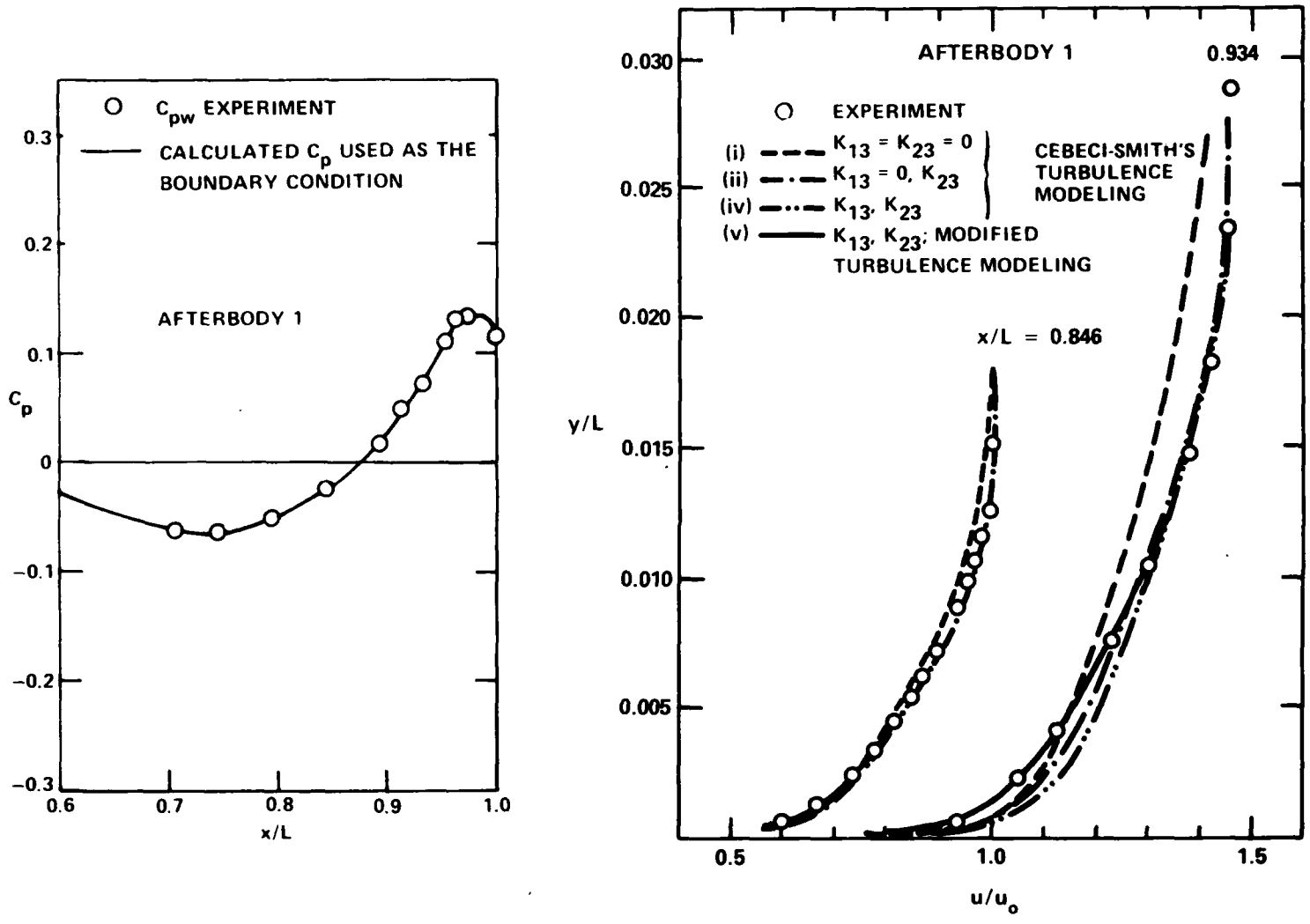

Figure 4a — Comparison in C_p and Velocity Profiles for Afterbody 1

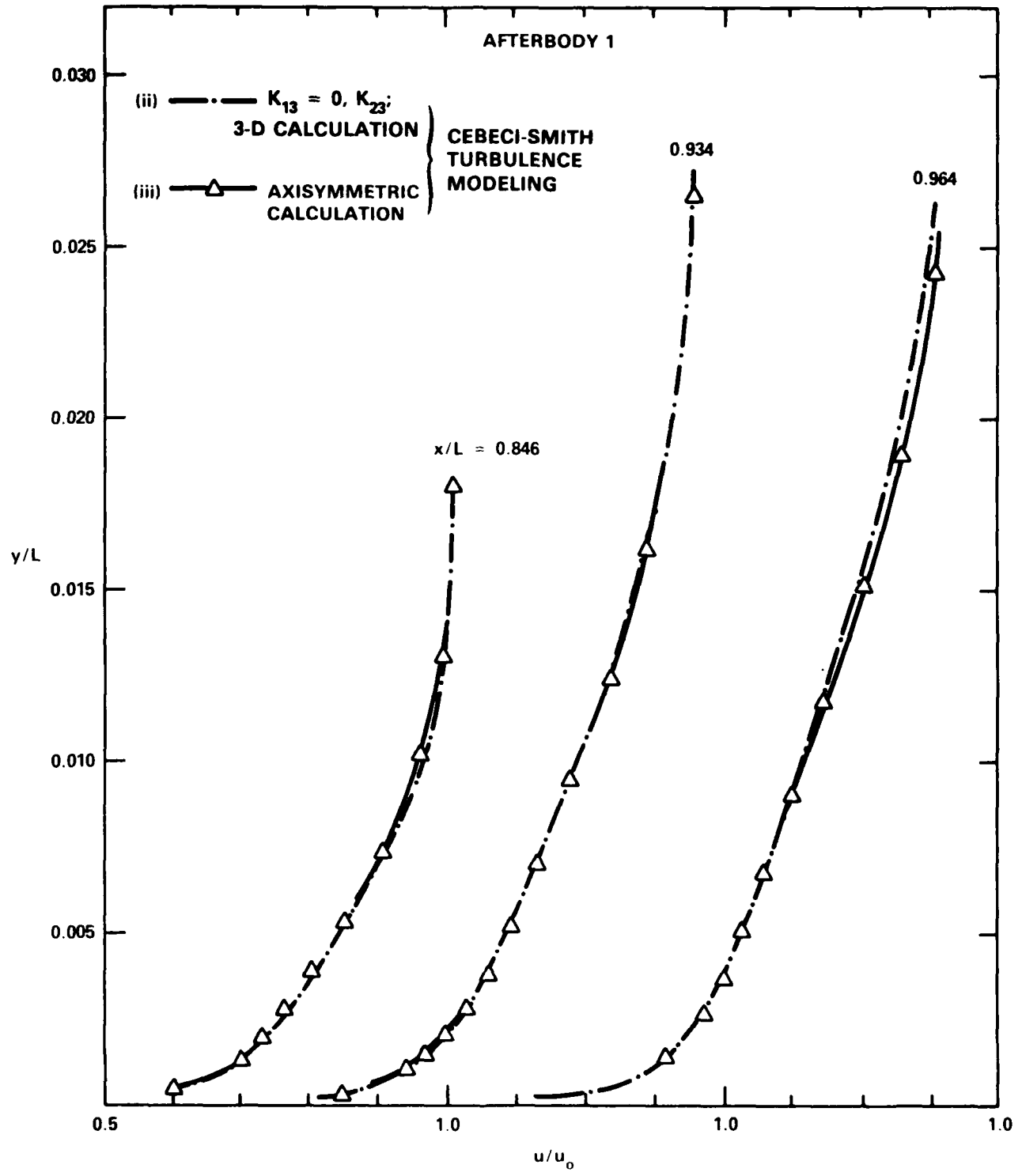

Figure 4b — Axisymmetric and 3-D Velocity Predictions for Afterbody 1

(iv) Modified turbulence model

(v) Huang's turbulence model (v)

The potential flow solution was obtained by using the XYZ potential flow code,[23] which utilizes Hess-Smith's method[24]. Calculation methods (i) and (ii) show the effect of the thick boundary layer, and calculation methods (ii) and (iii) show the effect of the added curvature terms. The results of the last three calculations illustrate the significance of the turbulence modeling.

Figure 5 shows plots of two different calculated C_p distributions used as the boundary conditions C_{pw} and C_{pe}. Measured values of C_{pw} and C_{pe} are also shown in Figure 5 for comparison. Although the measured data vary from station to station, this figure indicates that the pressure variation across the boundary layer becomes large when θ increases. The calculated C_{pe} values agree reasonably well with the measured C_{pe} values. The calculated C_{pw} values, however, have too strong a girth-wise adverse pressure gradient for θ between 80° and 90°. This behavior is responsible for the earlier predicted separation, which will be discussed later. The predicted drop-off of C_{pe} values near $\theta = 90°$ and $x/L \geq 0.89$ is also associated with this earlier predicted separation. With the $C_{pw}$and C_{pe} values shown in Figure 5, the actual magnitudes of the crossflow velocities used in the computations introduced in Equations (13) and (14) are plotted in Figure 6. Although the experimental data are quite scattered, the predicted w_e values are somewhat larger than the measured values, except at $x/L = 0.719$ for the 3:1 body.

The predicted axial velocity profiles are shown in Figures 7a and 7b for the 2:1 body and Figures 8a and 8b for the 3:1 body. Results of calculation (ii) are shown in all figures as baselines for comparing the relative magnitudes of the predictions. Separation is predicted when flow reversal occurs in the axial direction and the calculation stops at the predicted separation point. Therefore, at each θ-value, no profile is plotted downstream of the separation point. Table 1 shows the predicted separation locations x_{sep} and θ_{sep} for each case as compared to the experimentally observed locations of separation for the 2:1 body and Table 2 for the 3:1 body. Calculation set (i) predicts early separation. The other four calculation sets predict the locations of separation inception within 3% of the observed values. Figure 3 indicates that at $x/L = 0.894$ the transverse curvature for axisymmetric Afterbody 1 equals those of the two 3-D bodies near $\theta = 80°$. As θ increases further, the curvature becomes larger for the two 3-D bodies. But the predicted velocity profiles in Figure 4 for axisymmetric Afterbody 1 respond more strongly to the curvature effect than those in Figures 7 and 8 for the two 3-D bodies. This is due to the three dimensionality of the latter predictions.

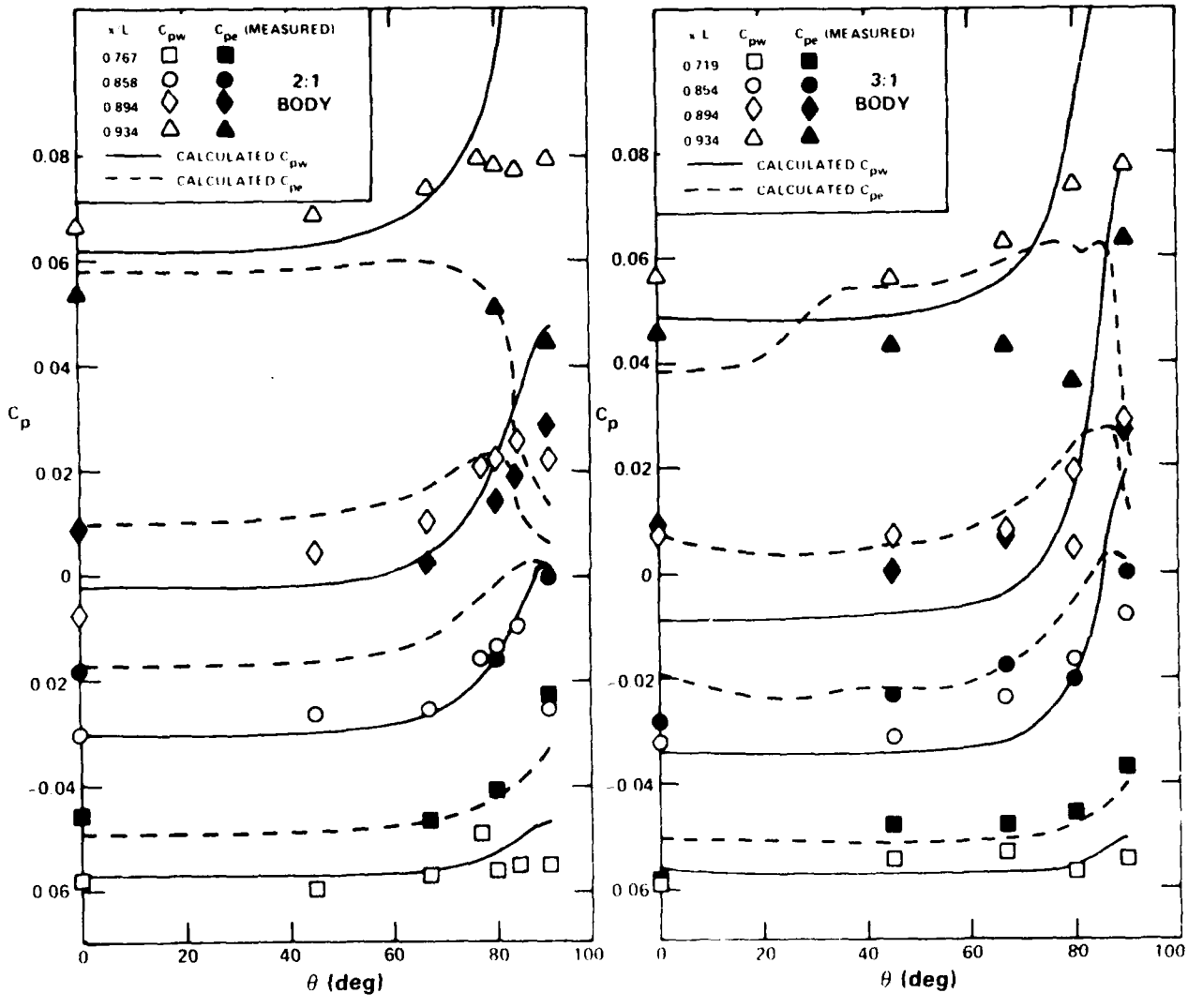

Figure 5 — Comparison in Pressure Coefficient

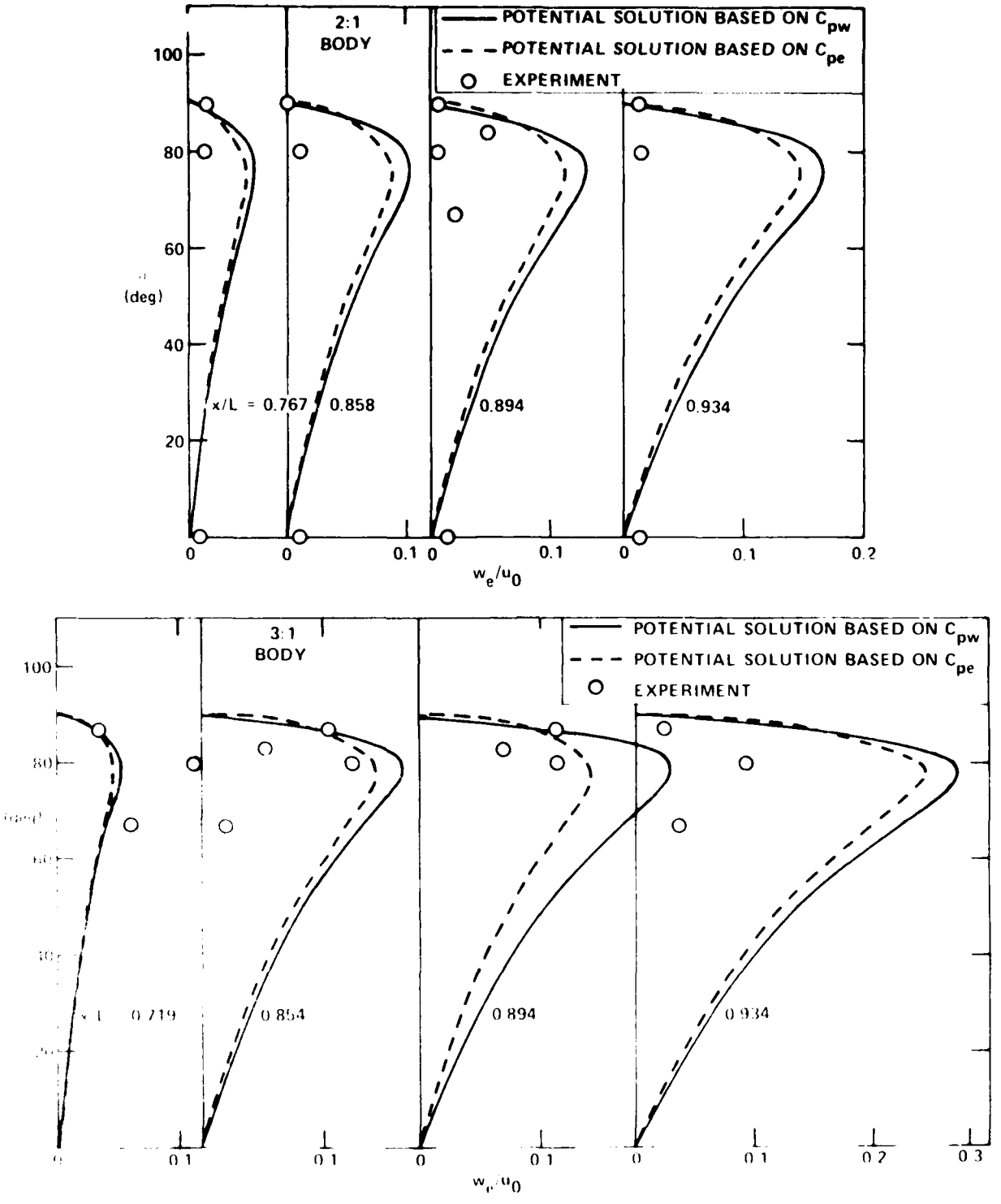

Figure 6 Comparison of Crossflow Condition at Edge of Boundary Layer

Figure 7 – Axial Velocity Predictions for the 2:1 Body

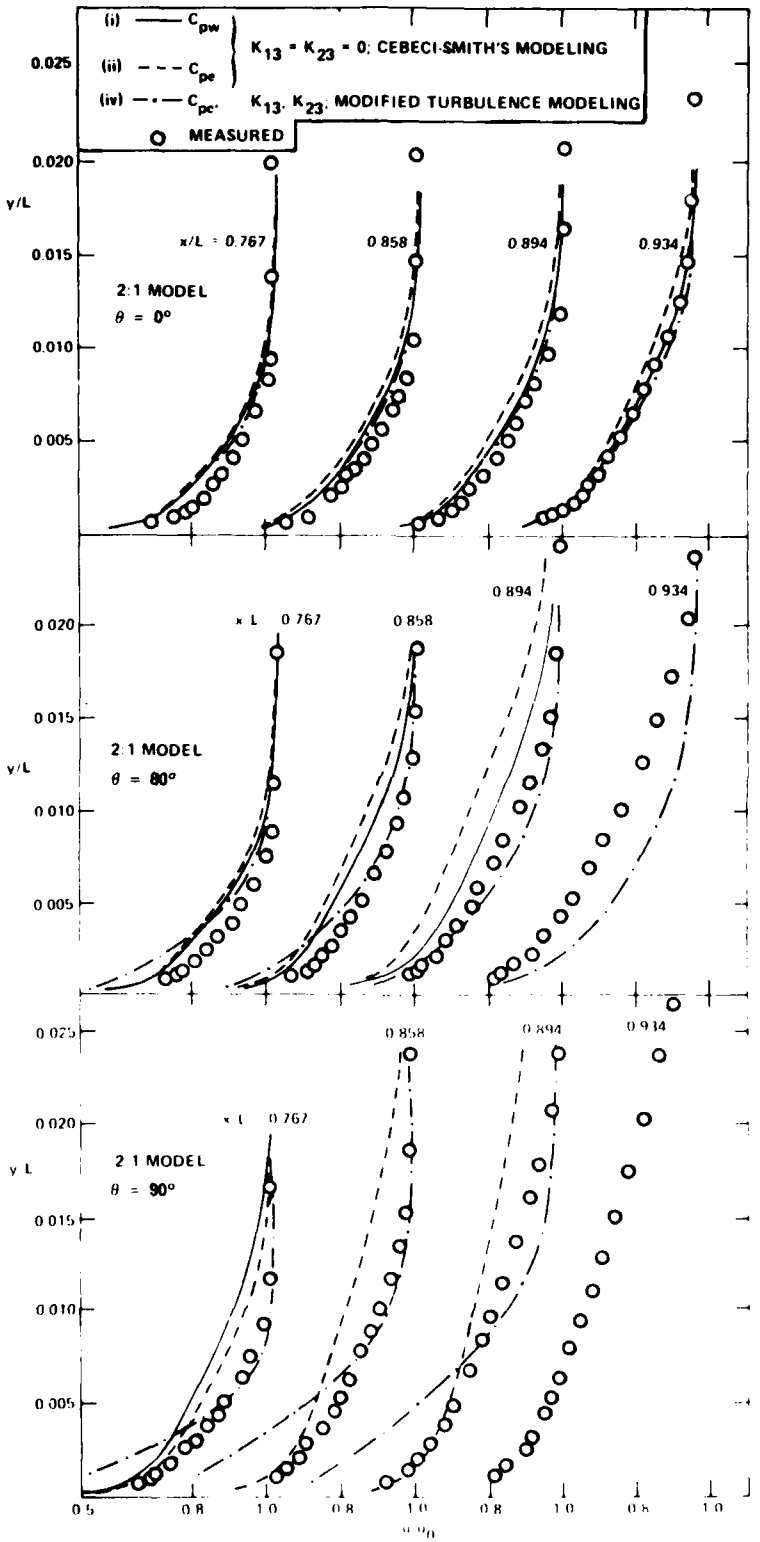

Figure 7a

Figure 7 (Continued)

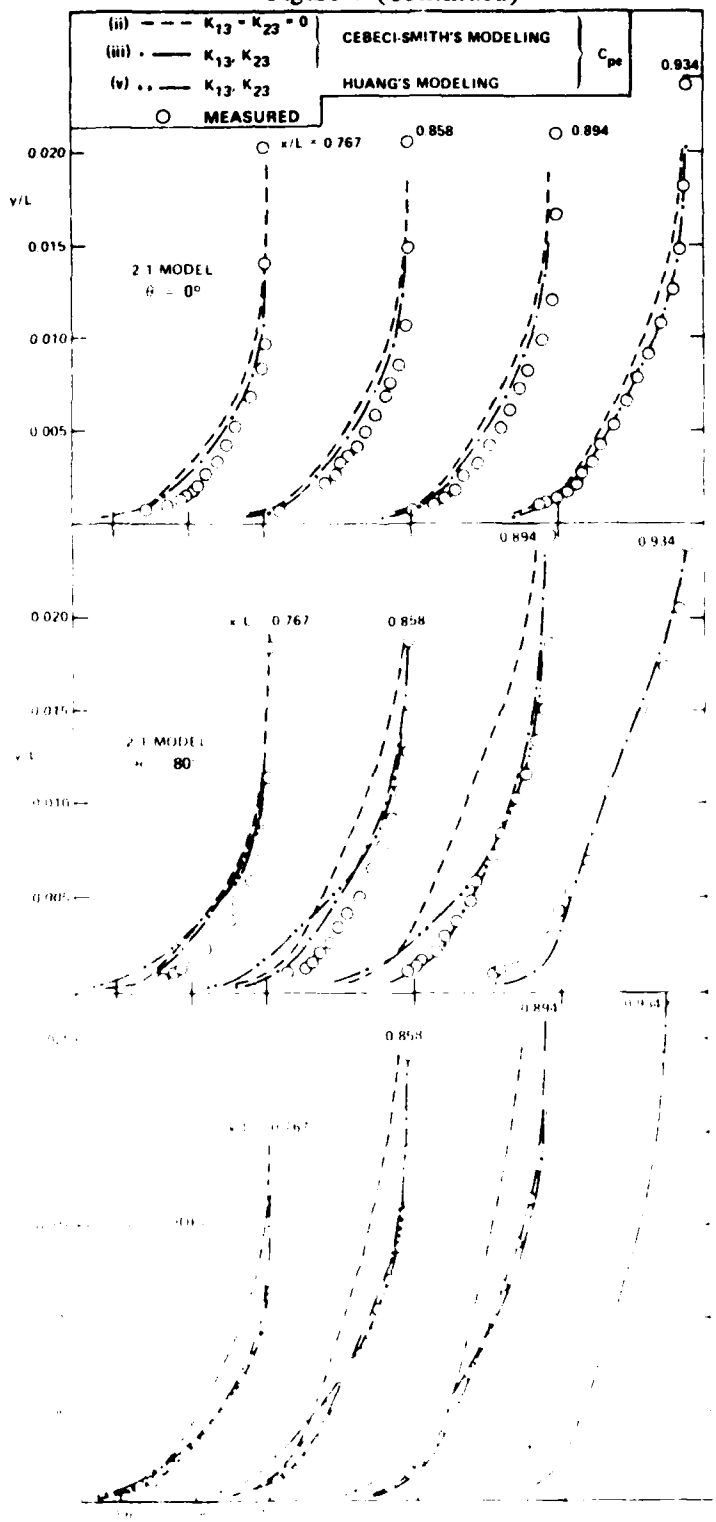

Figure 7b

Figure 8 – Axial Velocity Predictions for the 3:1 Body

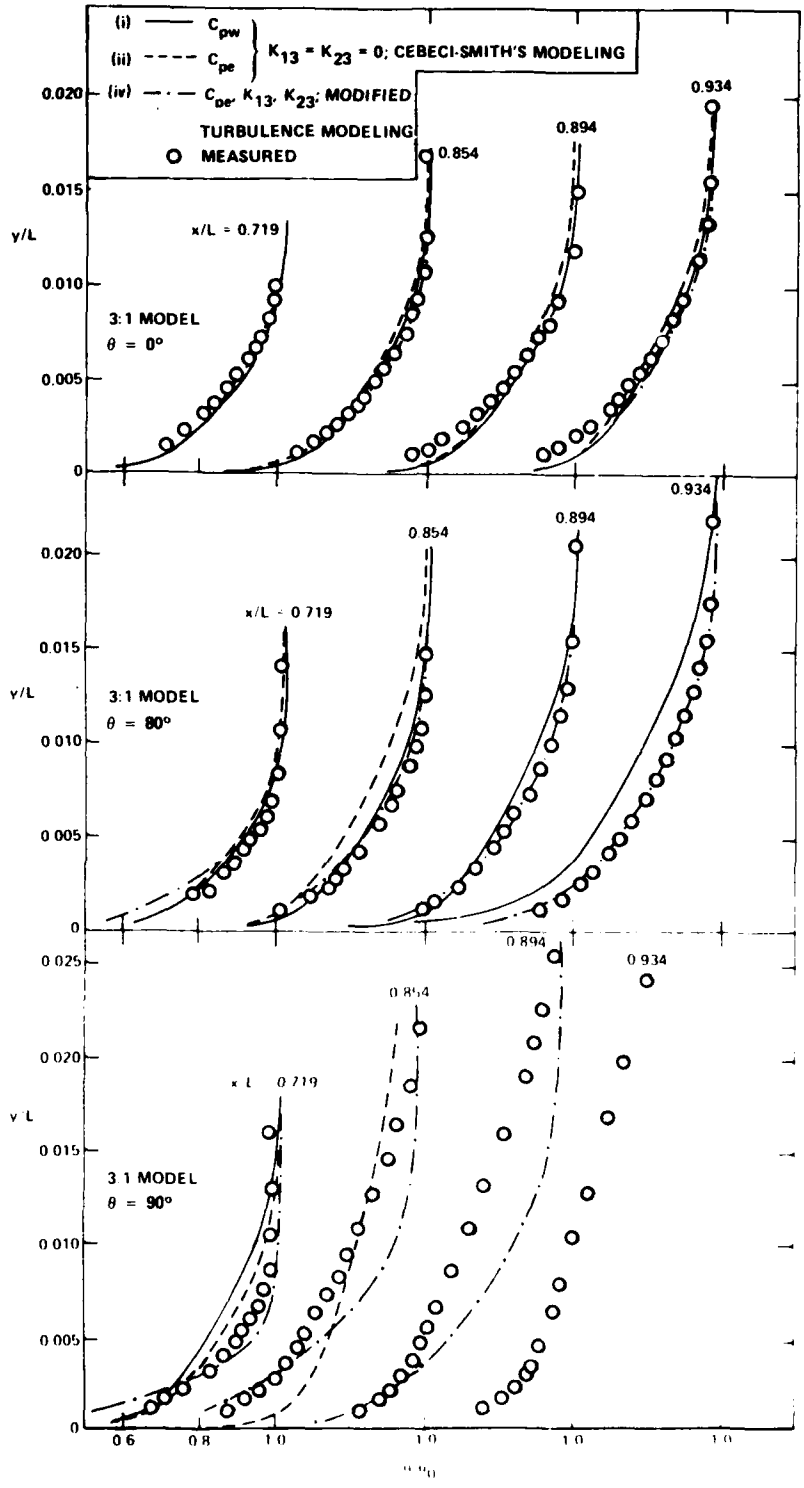

Figure 8a

Figure 8 (Continued)

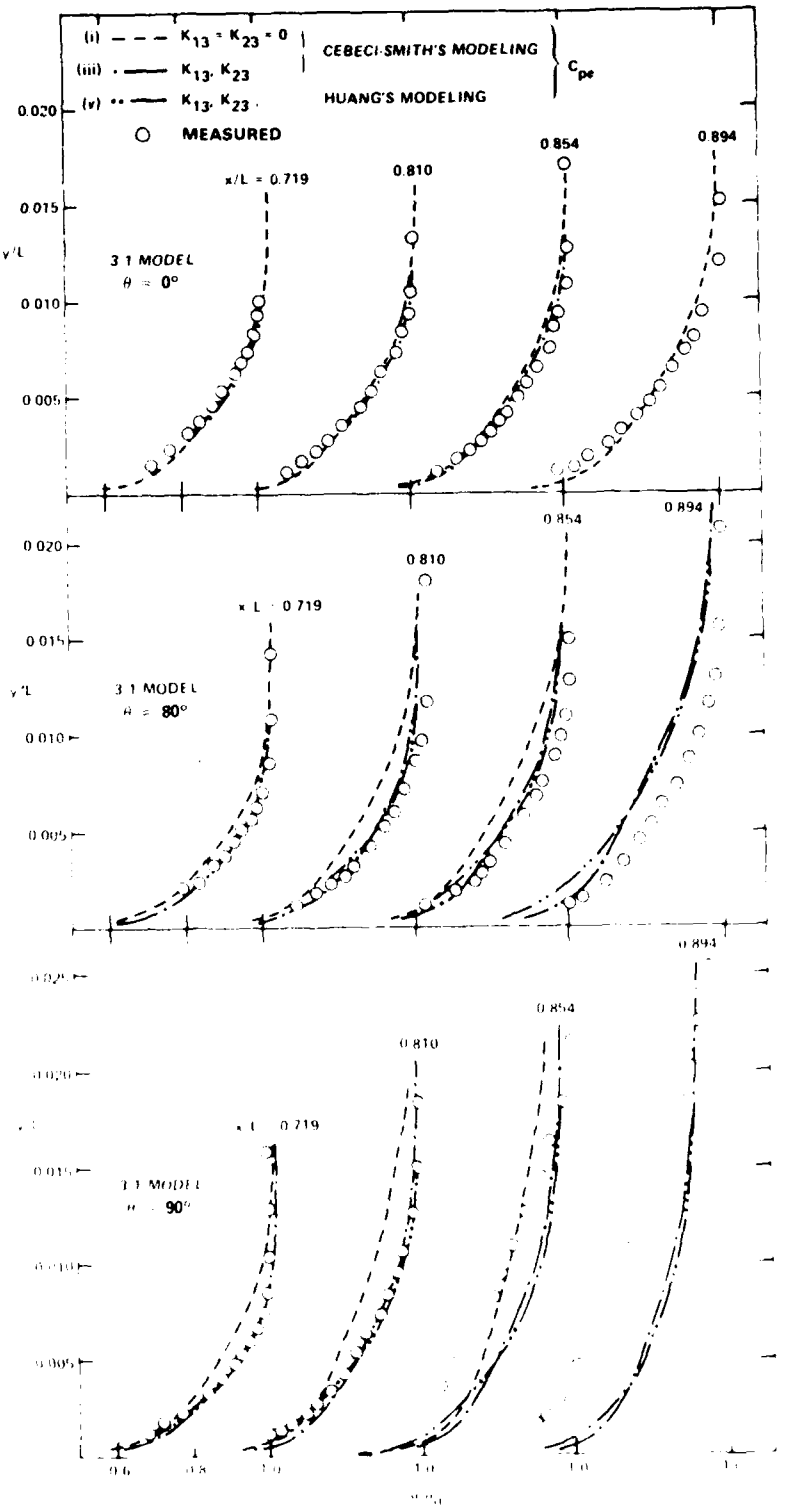

Figure 8b

TABLE 1 — PREDICTED LOCATIONS OF SEPARATION INCEPTION COMPARED TO THE EXPERIMENTAL OBSERVATION FOR THE 2:1 BODY

Boundary Condition	Curvature Effects	Turbulence Modeling	$(x/L)_{sep}$	θ_{sep}
Experiment			0.90	$80° \sim 90°$
Predictions				
(i) Wall	No	C-S*	0.775	90°
(ii) Edge	No	C-S	0.894	80.7°
(iii) Edge	Yes	C-S	0.934	83.2°
(iv) Edge	Yes	Modified	0.914	85.6°
(v) Edge	Yes	Huang	0.914	89.9°

*Cebeci-Smith

TABLE 2 — PREDICTED LOCATIONS OF SEPARATION INCEPTION COMPARED TO THE EXPERIMENTAL OBSERVATION FOR THE 3:1 BODY

Boundary Condition	Curvature Effects	Turbulence Modeling	$(x/L)_{sep}$	θ_{sep}
Experiment			0.92	$80° \sim 90°$
Predictions				
(i) Wall	No	C-S*	0.834	90°
(ii) Edge	No	C-S	0.934	75°
(iii) Edge	Yes	C-S	0.956	75°
(iv) Edge	Yes	Modified	0.934	85.6°
(v) Edge	Yes	Huang	0.907	90°

*Cebeci-Smith

The last three calculation sets for both 3-D bodies show the effect of turbulence modeling. Huang's turbulence model (calculation method (v)) underestimates the inner region velocity as compared to the Cebeci-Smith model (calculation method (iii)). Because of the overprediction of ℓ_1 in Equation (2) for the modified turbulence model, calculation method (iv) gives the worse predictions. This overprediction of ℓ_1 is related to the use of local curvature and boundary-layer parameters. Although the Cebeci-Smith turbulence model does not include curvature effects, it works better in terms of velocity prediction than the other two turbulence models for the two tested 3-D bodies. Figure 9 shows the eddy viscosity comparisons between the measured data and the calculated values by the Cebeci-Smith model and

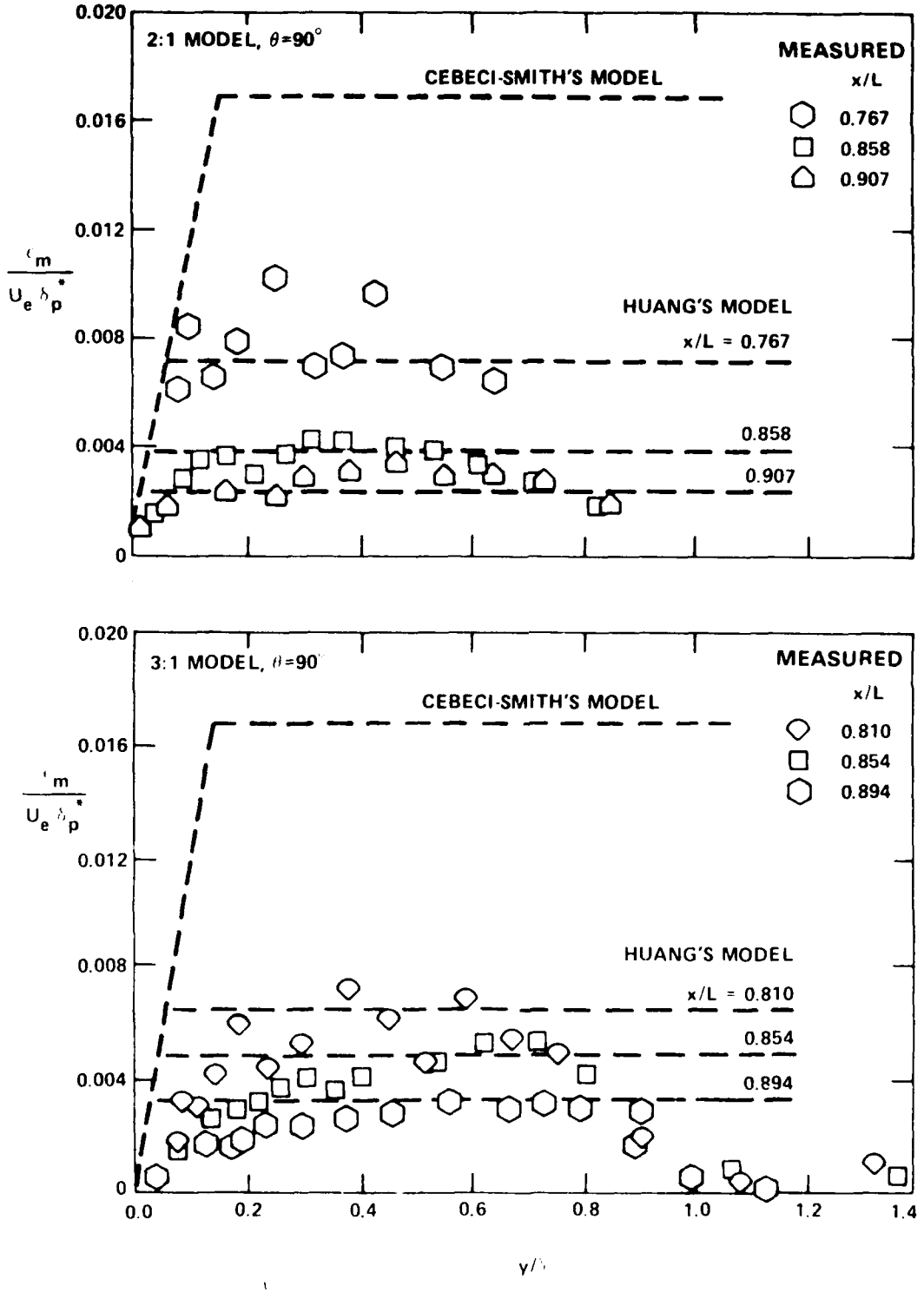

Figure 9 — Eddy Viscosity Comparisons

Huang's turbulence model (indicated by dashed line). Huang's turbulence model closely predicts the levels of the eddy viscosity in thick boundary layer, as compared to the measured data, but it underpredicts the velocity profile in the inner region unlike the Cebeci-Smith model.

Generally, the predictions of calculation method (iii), including the ones at x/L = 0.719 and 0.810, and θ = 90° for the 3:1 body, are in good agreement with the measurements. The deviation of the predicted velocity from the measured velocity at θ = 90° and x/L = 0.854; 0.894 for the 3:1 body in Figure 8 may be related to the proximity of the measurements to the separation point.

CONCLUSION

Three-dimensional thick boundary-layer equations, including variations of the metric coefficients, surface curvatures and static pressure coefficients with the normal distance from the wall, are solved by using the marching technique of Keller's box method. A nonorthogonal surface-fitted coordinate system is used. Formulas for calculating second-order geometric parameters are derived. Three turbulence models, two of which include the curvature effects, using the eddy-viscosity concept are compared. Three sets of measured data, for one axisymmetric and two 3-D flows are compared with calculated results. The conclusions drawn from the present study can be summarized as follows:

(i) The 3-D boundary-layer computations with varying geometric curvatures in the normal direction have been validated by comparing the axisymmetric boundary layer calculations to experimental data.

(ii) The predictions show a significant improvement in the present solution procedures by including the variation of transverse and longitudinal curvatures across the thick turbulent stern flows.

(iii) The calculation procedure that uses the edge boundary conditions (C_{pe}) for a thick boundary layer predicts a more accurate flow separation location for a separated flow than that using the surface boundary condition (C_{pw}).

(iv) The modified turbulence modeling, which uses the local curvature and local boundary-layer parameters, works reasonably well for axisymmetric flows but not as well for 3-D flow.

(v) Although Huang's turbulence model correlates eddy viscosity distributions in thick boundary layers better than the Cebeci-Smith model, the velocity predictions using Huang's model underestimate the inner-region velocity.

ACKNOWLEDGMENT

The authors wish to thank J.H. McCarthy and T.T. Huang for their continuous encouragement during the course of this research. Thanks are also due to N. Groves at DTNSRDC and K.C. Chang at the Douglas Aircraft Company for their consultation about the usage of the Douglas boundary-layer program.

APPENDIX

DERIVATION OF INNER-LAYER EDDY-VISCOSITY EQ. (19)

For a small pressure gradient flow, the x- and z-momentum Equations (9) and (10) in the inner region of the viscous layer can be approximated by

$$\frac{\partial}{\partial y}(h_1 h_2 \tau_s) = \frac{\partial}{\partial y}(h_1 h_2 \tau_z) = 0 \tag{A.1}$$

Integrating Equation (A.1) leads to

$$\alpha_1 \alpha_2 \tau_s = \tau_{sw} = \rho u_\tau^2 \tag{A.2}$$

The subscripts s and w stand for the streamline direction and the wall. By introducing the following nondimensional quantities,

$$u^+ = \frac{u_s}{u_\tau} \quad , \quad y^+ = \frac{y u_\tau}{\nu} \quad , \quad \varepsilon_m^+ = \frac{\varepsilon_m}{\nu}$$

$$K_{130}^+ = \frac{K_{130}\,\nu}{u_\tau} \quad , \quad K_{230}^+ = \frac{K_{230}^+\,\nu}{u_\tau} \tag{A.3}$$

$$\alpha_1^+ = \alpha_1 \quad , \quad \alpha_2^+ = \alpha_2$$

and by means of the eddy-viscosity concept, the Equation (A.2), in the fully turbulent flow, can be written in the nondimensional form as

$$\frac{du^+}{dY^+} + \varepsilon_m^+ \frac{du^+}{dY^+} = 1 \tag{A.4}$$

where

$$Y^+ = \begin{cases} \dfrac{\ln(\alpha_2^+/\alpha_1^+)}{K_{230}^+ - K_{130}^+} & , \quad \alpha_1^+ \neq \alpha_2^+ \\ \dfrac{y^+}{\alpha_2^+} & , \quad \alpha_1^+ = \alpha_2^+ \end{cases}$$

By comparing Equation (A.4) to the formulation of the eddy viscosity as shown in Reference 12 for 2-D flows, Equation (19) can be obtained.

REFERENCES

1. Larson, L., "SSPA-ITTC Workshop on Ship Boundary Layers 1980," Proceedings, The Swedish Maritime Research Center, (1981).

2. Abdelmequid, A.M., N.C. Markatos, K. Muraoka, and D.B. Spalding, " A Comparison Between the Parabolic and Partially-Parabolic Solution Procedures for Three Dimensional Turbulent Flows Around Ship's Hulls." Appl. Math Modelling, Vol. 3, p.249 (1982).

3. Muraoka, K., "Calculation of Thick Boundary Layer and Wake of Ships by a Partially Parabolic Method," Proc. 13th Symposium on Naval Hydrodynamics, Tokyo, p. 601 (1980).

4. Chen, H.C. and V.C. Patel, "Calculation of Stern Flows by a Time-Marching Solution of the Partially-Parabolic Equations," Proc. 15th Symposium on Naval Hydrodynamics, Hamburg (1984).

5. Larson, L. and M.S. Chang, "Numerical Viscous and Wave Resistance Calculations Including Interaction," Proc. 13th Symposium on Naval Hydrodynamics, Tokyo, p.707 (1980).

6. Soejima, S., "Calculation of Three-Dimensional Boundary Layers Around Ship Hull Forms," Proc. 2nd Symposium on Num. and Phys. Asp. of Aerody. Flows, Long Beach (1983).

7. Cebeci, T., K.C. Chang and K. Kaups, "A General Method for Calculating Three-Dimensional Laminar and Turbulent Boundary Layers on Ship Hulls," Douglas Aircraft Co., Report No. MDC J7998 (1978).

8. McDonald, H. and W.R. Briley, "A Survey of Recent Work on Interacted Boundary-Layer Theory for Flow With Separation," Proc. 2nd Symposium on Num. and Phy. Asp. of Aerody. Flows, Long Beach (1983).

9. Halsey, N.D., "Potential Flow Analysis of Multiple Bodies Using Conformal Mapping," M.S. Thesis, Dept. Mech. Eng., Calif. State Univ. at Long Beach (1977).

10. Nash, J.F. and V.C. Patel, "Three Dimensional Turbulent Boundary Layers," SBC Technical Books, Scientific and Business Consultants, Inc., Atlanta (1972).

11. Chen, K.L. and N.A.O. Thyson, "Extension of Emmon's Spot Theory to Flows on Blunt Body," J. of American Institute of Aeronautics and Astronautics, Vol. 9, No. 5 (1971).

12. Cebeci, T. and Smith, A.M.O., "Analysis of Turbulent Boundary Layers," Appl. Math and Mech., Vol 15, Academic Press p. 221. (1974)

13. Huang, T.T., N. Santelli, and G. Belt, "Stern Boundary Layer Flow on Axisymmetric Bodies," Proc. 12th Symposium on Naval Hydrodynamics, Washington, D.C., p. 127 (1978).

14. Wang, H.T. and T.T. Huang, "Calculation of Potential Flow/Boundary-Layer Interaction on Axisymmetric Bodies," ASME-CSME Apl. Mech. Fluids Eng. and Bioeng. Conference, Niagara Falls (1979).

15. Groves, N.C., G.S. Belt, and T.T. Huang, "Stern Boundary-Layer Flow on a Three-Dimensional Body of 3:1 Elliptic Cross Section," DTNSRDC Rep. 82/022 (1982).

16. Huang, T.T., N.C. Groves, and G.S. Belt, "Stern Boundary-Layer Flow on a Three-Dimensional Body of 2:1 Elliptic Cross Section." DTNSRDC Rep. 84/022 (1984).

17. Huang, T.T., "Measured Similarity Properties of Eddy Viscosity and Mixing Length in Three-Dimensional Turbulent Stern Flows," Proc. 2nd International Symposium on Ship Viscous Resistance, March 18 to 20, Gothenburg, Sweden (1985).

18. Cebeci, T. and P. Bradshaw, *Momentum Transfer in Boundary Layers,* McGraw-Hill (1977).

19. Lighthill, M.J., "On Displacement Thickness," J. of Fluid Mechanics, Vol. 4, Part 4 (1958).

20. Hoekstra, M. and H.C. Raven, "Calculation of Viscous-Inviscid interaction in the Flow Past a Ship Afterbody," Proc. 13th Symposium on Naval Hydrodynamics, Tokyo, pp. 585-598 (1980).

21. Nagamatsu, T., "Calculation of Ship Viscous Resistance by Integral Method and Its Application," Proc. 2nd International Symposium on Ship Viscous Resistance, March 17-20 (1985).

22. Cebeci, T., "A Computer Program for Calculating Incompressible Laminar and Turbulent Boundary Layers on Plane and Axisymmetric Bodies with Surface Roughness," Dept. of Mechanical Engineering, Calif. State Univ., Long Beach, Rep. No. TR-78-1 (1978).

23. Dawson, C.W. and J.S. Dean, "The XYZ Potential Flow Program," DTNSRDC Rep. 3892 (1972).

24. Hess, J.L. and Smith A.M.O., "Calculation of Potential Flow About Arbitrary Bodies," Prog. in Aeronautical Science, Vol.8, Pergamon Press Series (1966).

Initial Distribution

Copies

1 WES

1 U.S. ARMY TRANS R&D
Marine Trans Div

3 ONR/432F Whitehead,
Lee, Reishman

1 ONR/Boston

1 ONR/Chicago

1 ONR/New York

1 ONR/Pasadena

1 ONR/San Francisco

2 NRL
1 Code 2027
1 Code 2629

1 NORDA

3 USAN
1 Tech Lib
1 Nav Sys Eng Dept
1 B. Johnson

3 NAVPGSCOL
1 Lib
1 T. Sarpkaya
1 J. Miller

1 NOSC/Lib

1 NCSC/712

1 NCEL/131

1 NSWC, White Oak/Lib

1 NSWC, Cahlgren/Lib

1 NUSC/Lib

11 NAVSEA
1 SEA 05R24 (F. Ventrigho)
1 SEA55W3 (E. Comstock)
1 SEA 55W33 (W. Sandburg)
1 SEA 55W31 (W. Louis)

Copies

1 SEA 55W31 (G. Jones)
1 SEA 55N2 (A. Paladino)
1 SEA 55N1 (S.G. Wieczorek)
1 SEA 63R31 (T. Peirce)
1 SEA 56X12 (C.R. Crockett)
1 SEA 62R41 (L. Pasiuk)
1 SEA 99612 (Library)

1 NAVFAC/032C

1 NADC

1 NAVSHIPYD PTSMH/Lib

1 NAVSHIPYD PHILA/Lib

1 NAVSHIPYD NORVA/Lib

1 NAVSHIPYD CHASN/Lib

1 NAVSHIPYD LBEACH/Lib

2 NAVSHIPYD MARE
1 Lib
1 Code 250

1 NAVSHIPYD PUGET/Lib

1 NAVSHIPYD PEARL/Code 202.32

1 NAVSEC, NORVA/6660.03, Blount

12 DTIC

1 AFORSR/NAM

1 AFFOL/FYS, J. Olsen

2 MARAD
1 Div of Ship R&D
1 Lib

1 NASA/HQ/Lib

3 NASA/Ames Res Ctr, Lib
1 D. Kwak
1 J.L. Steger
1 Lib

2 NASA/Langley Res Ctr
1 Lib
1 D. Bushnell

Copies	
1	NBS/Lib
1	LC/Sci & Tech
1	DOT/Lib TAD-491.1
2	MMA 1 National Maritime Res Ctr 1 Lib
3	U of Cal/Dept Naval Arch, Berkeley 1 Lib 1 W. Webster 1 R. Yeung
2	U of Cal, San Diego 1 A.T. Ellis 1 Scripps Inst Lib
1	U of Cal, Santa Barbara/Tulin
4	CIT 1 Aero Lib 1 T.Y. Wu 1 A.J. Acosta 1 D. Coles
1	California State University/Cebeci
1	Cathelic U of Amer/Civil & Mech Eng
1	Colorado State U/Eng Res Ctr
1	Cornell U/Shen
2	Harvard U 1 G. Carrier 1 Gordon McKay Lib
1	U of Illinois/J. Robertson
4	U of Iowa 1 Lib 1 L. Landweber 1 V.C. Patel 1 C.J. Chen
1	Johns Hopkins U/Lib

Copies	
4	MIT 1 Lib 1 J.R. Kerwin 1 T.F. Ogilvie 1 J.N. Newman
2	U of Minn/St. Anthony Falls 1 Lib 1 Arndt
1	U of Mich/NAME/Lib
1	U of Notre Dame/Eng Lib
1	New York U/Courant Inst/Lib
3	Penn State 1 B.R. Parkin 1 R.E. Henderson 1 ARL Lib
1	Princeton U/Mellor
1	U of Rhode Island/F.M. White
1	Science Applications, Inc. Annapolis, MD C. von Kerczek
1	SIT/Lib
1	U of Texas/Arl Lib
1	Utah State U/Jeppson
1	Southwest Res Inst 1 Applied Mech Rev
3	Stanford U 1 Eng Lib 1 R. Street, Dept Civil Eng 1 S.J. Kline, Dept Mech Eng
1	Stanford Res Inst/Lib
1	U of Virginia/Aero Eng Dept
1	U of Washington/Arl Tech Lib

Copies	
2	VPI 1 Dept of Mech Eng 1 J. Schetz, Dept Aero & Ocean Eng
2	Webb Inst 1 Lib 1 Ward
1	Woods Hole/Ocean Eng
1	Worchester PI/Tech Lib
1	SNAME/Tech Lib
1	Bell Aerospace
1	Bethlehem Steel/Sparrows Point
1	National Science Foundation/Eng Div Lib
1	Bethlehem Steel/New York/Lib
4	Boeing Company/Seattle 1 Marine System 1 P. Rubbert 1 G. Paynter 1 H. Yoshihara
1	Bolt, Beranek & Newman/Lib
1	Cambridge Acoustical Associates, Inc.
1	Exxon, NY/Design Div/Tank Dept
1	Exxon Math & System, Inc.
1	General Dynamics, EB/Boatwright
1	Flow Research
1	Gibbs & Cox/Tech Info
2	Grumman Aerospace Corp 1 Lib 1 R.E. Melnik
1	Hydronautics/Lib
1	Lockheed, Sunnyvale/Waid

Copies	
1	Lockheed, California/Lib
1	Lockheed, Georgia/Lin
2	McDonnell Douglas, Long Beach 1 T. Cebeci 1 J.L. Hess
1	Newport News Shipbuilding/Lib
1	Nielsen Eng & Research
1	Northrop Corp/Aircraft Div
1	Rand Corp
1	Rockwell International 1 B. Ujihara
1	Sperry Rand/Tech Lib
1	Sun Shipbuilding/Chief Naval Arch
1	TRW Systems Group/Lib
1	TRACOR
1	United Technology/East Hartford, Conn
2	Westinghouse Electric 1 M.S. Macovsky 1 Gulino

CENTER DISTRIBUTION

Copies	Code	Name
1	012.3	D.D. Moran
1	1500	W.B. Morgan
1	1504	V.J. Monacella
1	1506	S.Hawkins
1	1508	R. Boswell
1	152	W.C. Lin
1	1521	W. Day

CENTER DISTRIBUTION

Copies	Code	Name
1	154	J.H. McCarthy
1	154	P. Granville
1	1542	T.T. Huang
1		N.C. Groves
15		Y.T. Lee
1		M.S. Chang
1		F. Noblesse
1		D. Hendrix
1	1544	F. Peterson
1	156	D.S. Cieslowski
1	1561	G. Cox
1	1564	J. Feldmen
1	1606	T.C. Tai
1	1802.1	H. Lugt
1	1840	J. Schot
1	1843	H. Haussling
1		H. Cheng
1	19	M.M. Sevik
1	1905.1	W. Blake
1	194	F.S. Archibald
10	5211.1	Reports Distribution
1	52.1	TIC (C)
1	522.2	TIC (A)

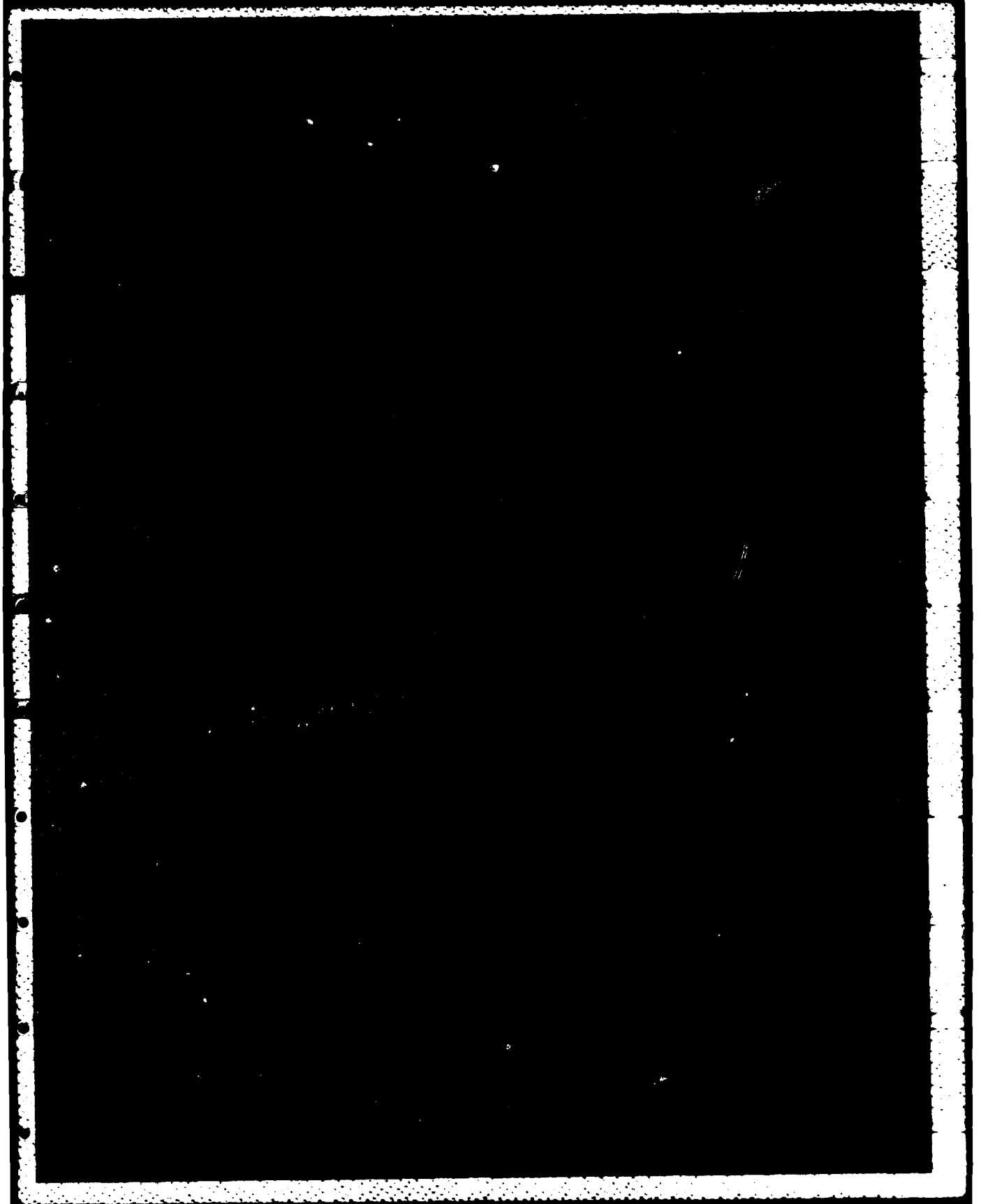

END

FILMED

2-86

DTIC